A Stark Future for Quantum Control

Dave Townsend,*,† Benjamin J. Sussman,‡ and Albert Stolow‡

School of Engineering and Physical Sciences, Heriot-Watt University, Edinburgh, EH14 4AS, United Kingdom, and Steacie Institute for Molecular Sciences, National Research Council of Canada, 100 Sussex Drive, Ottawa, Ontario, K1A 0R6, Canada

Received: September 23, 2010; Revised Manuscript Received: November 15, 2010

We present an overview of developments using the nonresonant dynamic Stark effect within the fields of time-resolved molecular dynamics and quantum control, drawing on examples from our own recent work. Particular emphasis is placed on the notion that "dynamics" and "control" are not distinct disciplines and that a clear synergy exits between these areas which has, up to now, been somewhat underexploited. The dynamic Stark effect is a universal interaction which we expect to have broad applicability.

Introduction

The static and dynamic behavior of electrons and atomic nuclei determines the properties of all molecular systems. The electromagnetic forces driving such behavior ultimately impose limits on the feasibility and rates of all molecular processes and therefore underpin all of chemistry (and, by extension, biology). A natural approach to exerting control over atomic and molecular systems is therefore through the application of externally applied electromagnetic fields. The electromagnetic fields created by modern lasers generate forces comparable to those that bind atoms and molecules and can do so on the natural time scales of their motions. Consequently, lasers offer an ideal tool for effecting control over molecular processes, and achieving this goal has become one of the "grand challenges" within the field of chemistry over the past three decades.[1−11]

From a chemical point of view, an understanding of dynamical behavior may be formulated in terms of the various mechanistic pathways that connect an initial set of states (or reactants) to a final set of states (or products). The study of chemical dynamics is therefore often concerned with developing an understanding of the detailed evolution of the electronic and nuclear degrees of freedom as the reaction coordinate connecting reactants to products is traversed. Implicitly, this is the study of the electrical forces present in the system.

A commonly cited notion of chemical control centers around the desire to precisely manipulate the relative yields of the various product states that may be formed in a given reaction process, that is, to influence rather than just passively observe the dynamics. However, even in the absence of any control strategy, the dynamics of many molecular processes are not well understood. This has served as a strong motivating factor in the development of increasingly sophisticated or "differential" experimental techniques to study dynamical processes. As we shall discuss in more detail below, the use of externally applied electromagnetic control fields can also be used to further enhance the differential nature of these observation-based measurements, for example, by preparing a specific state before a measurement rather than starting with a thermal distribution. As such, the notions of observing and controlling molecular dynamics are strongly connected. Control may lead to improved observation and hence better dynamical understanding. Improved understanding of the system dynamics may then, in turn, ultimately lead to more refined strategies for control.

Observation

Our understanding of molecular structure and dynamics is based primarily on the Born−Oppenheimer (BO) approximation, which relies on the fact that nuclei are much heavier than electrons and therefore usually move more slowly. The nuclear motion (vibrations and rotations) may therefore be adiabatically separated from the motion of the electrons in the system, and this leads naturally to the concept of electronic energy landscapes (potential energy surfaces) determined by fast-moving electrons, over which the much slower nuclear motion evolves. This adiabatic approximation is central to enabling the discussion of dynamical processes to be framed in terms of a language which includes the concept of well-defined vibrational energy states, and it has proved very successful in modeling the behavior of simple molecules. Even in these simple systems, however, the coupling between the nuclear and electronic degrees of freedom is often not negligible, especially when electronically excited states are being considered. In the excited states of larger and more complex systems, there is growing evidence that these breakdowns of the BO approximation are, in fact, the rule rather than the exception.[12,13] They are also known to be central to biological function in fundamentally important processes such as vision and photosynthesis.[14−18] There is, therefore, a fundamental challenge to develop our understanding of non-BO dynamics for molecular systems and ultimately extend this to complex environments, such as solutions, bulk materials, liquid and solid surfaces, interfaces, and biological systems.

Deviations from the BO limit take on a variety of names when discussed within the field of molecular dynamics. Nonadiabatic processes, radiationless transitions, internal conversion, electronic relaxation, curve crossing, and conical intersection may all, however, be interpreted as a coupling (i.e., energy transfer) between the electronic and nuclear degrees of freedom (as described by the initial BO picture) within the evolving chemical system. Over the past four decades or more, the development of techniques to probe the role of these processes with an ever-increasing level of detail has been central to furthering the understanding of chemical dynamics.

* To whom correspondence should be addressed.
† Heriot-Watt University.
‡ National Research Council of Canada.

10.1021/jp109095d
Published on Web 12/23/2010

Dave Townsend is currently a lecturer at Heriot-Watt University in Edinburgh, with research interests in the area of time-resolved molecular spectroscopy and dynamics. Dave began his university career studying chemistry as an undergraduate at the University of Nottingham, where he then remained to undertake a Ph.D. with Prof. Katharine Reid, studying angle-resolved photoionization dynamics of polyatomic molecules. Following on from this, he spent time as a postdoctoral researcher at the University of Oxford with Prof. Tim Softley, investigating the translational control of atomic and molecular Rydberg states, and then studied in the group of Prof. Arthur Suits at SUNY Stony Brook, using imaging methods to study vector correlations in molecular photodissociation. Between 2004 and 2007, he was a Visiting Fellow at the National Research Council of Canada in Ottawa.

Benjamin Sussman is a Research Officer in the Steacie Institute for Molecular Sciences at the National Research Council of Canada and a Research Fellow at Worcester College, University of Oxford. His research investigates the intersection of quantum control, quantum information, and photonics. He studied physics as an undergraduate at the University of Waterloo before obtaining his M.Sc. at the University of British Columbia. He graduated with a Ph.D. in Physics from Queen's University in 2007.

Albert Stolow studied chemistry and physics at Queen's University. He then obtained his Ph.D. from the University of Toronto, studying under John C. Polanyi. Albert was then an NSERC postdoctoral fellow with Yuan T. Lee at the University of California, Berkeley, where he became interested in the dynamics of polyatomic molecules. In 1992, he joined the Femtosecond Science Program of the Steacie Institute for Molecular Sciences (National Research Council of Canada) to begin research in the area of femtosecond dynamics based on time-resolved photoelectron spectroscopy. Albert is currently a Principal Research Officer within the Steacie Institute for Molecular Sciences and Program Leader of the Molecular Photonics Group. He is Adjunct Professor of Chemistry and Adjunct Professor of Physics at Queen's University and Adjunct Professor of Physics at the University of Ottawa. His group's research interests include ultrafast molecular dynamics and quantum control, nonlinear optical spectroscopy, molecular strong-field physics, and nonlinear microscopy of live cells. He is a Fellow of both the American Physical Society and the Optical Society of America, has won several prizes, including the Keith Laidler Award of the Chemical Society of Canada, and sits on the editorial boards of various international journals.

"Zero-order" measurements such as the simple observation of product yields from a given chemical process are clearly insufficient to infer much dynamical information. With a little more effort on the part of the experimenter, however, improved "first-order" observations, for example, the energy partitioning among the internal degrees of freedom within the reactants and products, may begin to provide some degree of insight into the transit along the reaction coordinate, as illustrated, for example, in the classic "early" and "late" barrier pictures for chemical reactions.[19,20] In order to take this line of investigation further, even higher-order, or increasingly differential, measurements are required. As a first step up this ladder of experimental complexity, one may begin to consider the angular direction in which various products are ejected, or scattered, with respect to a given frame of reference. In the laboratory frame, this is typically taken to be the polarization vector of a laser pulse that initiates a (unimolecular) photochemical process or the axis along which a (bimolecular) collision between reactant species takes place. As a next step, one may then begin to correlate energy- and angle-resolved information, investigating the variation in product internal energy as a function of scattering angle. The multiplexing advantages offered by the advent of position-sensitive, 2D imaging methods over the past two decades made such a task a readily viable experimental undertaking.[21,22] Correlated measurements of this type begin to reveal many subtle details of the transit along the reaction coordinate connecting reactants to products. However, one may still go further in an attempt to develop an even more complete picture. In addition to the recoil velocity of the products, there are other vector properties present in the system, specifically, the various angular momenta in the products, that may exhibit significant polarization anisotropy. The ability to not only measure this anisotropy but to correlate it with the recoil velocity offers a powerful probe of the overall dynamics.[23−29] Vector correlations of rotational angular momentum polarization in molecular photofragments provide much information on the shape of the potential energy surfaces involved in the evolution from reactants to products. Observations of electronic angular momentum polarization in atomic photofragments are perhaps even more powerful, yielding insight into the coupling (and associated phase shifts) between different potential energy surfaces involved in mediating the dynamics in molecular systems. This point is particularly apparent if one views the unpaired electrons in the recoiling photofragments as having previously formed part of the "fabric" of the potential energy surfaces in the system under study prior to dissociation. Finally, one may also consider photoelectron angular distributions (PADs) from photoionization. Such distributions are a superposition of many "partial waves" with different angular momenta, l, and the overall appearance of such distributions is highly sensitive to the amplitude and relative scattering phase of these various constituent components, in turn providing detailed information on the symmetry of the state from which ionization occurred.[30−33]

As a next step toward further improving the differential nature of dynamics experiments, one may begin to consider the possibility of making measurements in the molecular frame of reference rather than that of the laboratory frame. For the case of a simple photodissociation, these two frames are effectively commensurate, assuming that the time scale of fragmentation is fast compared to the period of molecular rotation, the so-called axial recoil limit. However, more sophisticated experimental approaches are often required to extract molecular frame information in many other types of processes. This includes systems that deviate from the axial recoil limit, systems that produce more than two fragments upon dissociation (including, for example, the cases of dissociative photoionization or photodetachment), and systems where dissociation is not a dominant mechanism. The use of multibody coincidence techniques[34] has been successfully demonstrated as a route to obtaining molecular frame measurements in some of these types of system.[35−40] A second strategy, which will form one of the main themes for discussion in this article, is to try to "overlap" the molecular and laboratory frames of reference through the use of externally applied aligning or orienting fields.

The development of modern laser sources has enabled experimentalists to develop approaches that seek to interrogate dynamical processes in chemical systems with increasingly high levels of precision. Broadly speaking, these approaches may be broken down into two main categories, time-resolved and frequency-resolved measurements. In the case of the latter, one is able only to probe the products formed in the asymptotic region of the reaction coordinate, owing to the long temporal duration of the laser pulses relative to the typical time scales of reaction dynamics. However, the narrow line width laser sources used in such measurements often enable the products to be probed in a quantum-state-specific manner. This high level of spectroscopic resolution is a powerful tool for enabling the dynamics of a chemical event to be inferred. In the case of time-resolved measurements, one is effectively able to follow the evolution of the system dynamics in real time as the reaction coordinate is traversed, but there is always a trade off in terms of spectroscopic resolution as the broader bandwidth associated with so-called "ultrafast" laser pulses means that quantum-state-specific measurements are not usually possible. This trade off of energy versus time resolution means that a combination of

different experimental approaches (both time- and frequency-resolved) are often required to develop a complete mechanistic picture; that is, there is no "one size fits all" approach, and data from a number of different, complementary techniques (with different associated observables) are often necessary. In the case of both time-resolved and frequency-resolved measurements, there are a vast number of different experimental techniques that may be employed and observables that may be monitored. Reflecting this, the field of molecular dynamics has grown enormously to encompass the detailed study of many types of molecular processes with ever-increasing degrees of sophistication. However, although hugely diverse in terms of scope and application, the vast majority of these dynamical studies are all bound together by one common feature, namely, that the observations are typically of a passive nature. In other words, the investigator sets a chain of dynamical events in motion and then either follows directly (time-resolved) or infers indirectly from the set of chemical outcomes (frequency-resolved) the mechanistic pathways connecting the set of initial and final states. While such studies are of huge importance in furthering our understanding of many fundamental processes, the next level of development within the field of molecular dynamics centers around the desire to move beyond this passive approach and into a regime where the dynamics are actively controlled.

Control

As discussed previously, electric forces underpin the dynamics of all chemical processes. In order to exert control over a chemical outcome, the use of additional, externally applied, electric fields is therefore a natural approach. This is not a new idea in many respects; the example of simple catalysis (for example, the case of adsorption on a metal surface) is one of externally applied fields (from the surface) being used to directly affect a chemical outcome by reducing the activation barrier along the reaction coordinate connecting the reactants to a specific set of products — the most commonly cited form of control when applied to molecular systems. However, externally applied static electromagnetic fields have also been used effectively as a form of "control" to enhance the otherwise passive observation of chemical processes, rather than modify the likelihood of a specific outcome per se. For example, the use of hexapole devices as well as so-called "brute-force" methods to select oriented neutral molecules has been employed in "stereodynamic" studies of bimolecular reactions.[41−44] This is effectively a form of control applied to the rotational degree of freedom, as will be expanded upon later. Other types of approach have also been used to exert control over the translational degree of freedom of neutral atoms and molecules via electrostatic interactions.

The first and perhaps most famous example of translational control over neutral species was the Stern−Gerlach experiment,[45] in which inhomogeneous magnetic fields were use to deflect a beam of silver atoms. Of the other, more recent approaches developed to control motion in neutral systems, perhaps the most well-known is the Stark decelerator developed by Meijer and co-workers,[46,47] which has found application in the rapidly growing area of cold molecule physics.[48] A very similar idea has also been explored by Softley and co-workers,[49−52] who have used the Stark effect as a tool to control translational motion in atomic and molecular Rydberg states in a manner analogous to that of the Meijer group. An important yet subtle difference in this approach is that, owing to the much larger Stark shifts exhibited by moderately high lying electronically excited Rydberg states (typically with principal quantum numbers in the $n = 10-20$ region), dramatically smaller field gradients (on the order of a few hundred V/cm rather than the kVs/cm required for ground-state systems) are all that is required to exert significant translational control. This increased magnitude of the Stark shift relative to that typically seen in ground electronic state configurations is a consequence of the linear rather than quadratic Stark shifts that result due to l degeneracy, as well as the inherently more polarizable nature of the loosely bound Rydberg electron. (There are no linear Stark shifts in nondegenerate states.) This issue of polarizability (both relative and absolute) will be an important consideration when we come, in subsequent sections, to examine the nonresonant dynamic Stark effect as a tool for control.

An alternative strategy to achieve control is through the use of externally applied coherent electromagnetic radiation, that is, laser light. This idea has been exploited for translational control using the Stark effect in a similar manner to that described above for static fields;[53−55] however, it is the use of laser fields for the direct control of chemical reactions that will form the central basis for the remainder of the brief discussion outlined here. Perhaps the first operational approach to controlling quantum states with external fields was given by Lamb in 1969.[56] Lamb argued that a practical discussion of quantum states should include a program for making them, and he offered such a method for producing arbitrarily shaped wave functions. The advent of intense, coherent laser sources extended the work of constructing arbitrary control, although initial hopes of achieving bond-selective chemistry through targeted resonant excitation of specific vibrational modes proved unsuccessful in the vast majority of cases, owing to the rapid statistical repartitioning of internal energy, the phenomenon commonly known as intramolecular vibrational energy redistribution (IVR).[57,58] More complex and subtle strategies for achieving chemical control using laser fields were therefore needed.

A renaissance in the field of laser control began in the 1980s with the work of Brumer and Shapiro,[1,59] who considered using quantum interference effects to manipulate chemical reactions. This was first experimentally demonstrated by Gordon and co-workers.[60] If two different laser-induced transitions to a specific target state occur with amplitudes $A_1 = |A_1|e^{i\varphi_1}$ and $A_2 = |A_2|e^{i\varphi_2}$, then the overall probability for populating that state is given by

$$P = |A_1|^2 + |A_2|^2 + 2|A_1||A_2| \cos(\phi_1 - \phi_2) \qquad (1)$$

The phases ϕ_1 and ϕ_2 may be independently controlled by altering the laser phases, and hence, the overall transition can be influenced. This coherent control approach is similar in some respects to Young's famous two-slit experiment where optical interference is observed due to multiple pathways to a screen; adding or subtracting a phase to one pathway has the effect of shifting the interference fringes. Within the coherent control approach, the "control" is mediated entirely by the laser phase that initiates a given photochemical event. The subsequent scattering phase then remains unaltered as the initially prepared reactant states evolve toward the products.

A second related approach to laser-induced control of photochemical processes was proposed by Tannor and Rice, who considered control over reactions that could form different reaction products in the ground electronic states of molecules.[4,61] Activation barriers were circumvented via other electronically excited states, where the absence of these barriers allowed free movement of a wavepacket to a target region of the potential

energy surface from which a transition back to the ground electronic state was initiated. In a sense, this so-called pump−dump control strategy may be viewed as a multiplexed or wavepacket version of the Brumer−Shapiro approach, where broad bandwidth laser pulses were used in the former and narrow line widths in the latter.

A number of approaches have investigated the application of adiabatically varied resonant laser fields. Perhaps the most well-known of these is stimulated Raman adiabatic passage (STIRAP), which is typically utilized in a three-level lambda system, where a resonant field connects the ground state with the intermediate state and a second resonant field connects the intermediate state with the target state. The eigenstates of the rotating wave Hamiltonian can be solved analytically and have a solution that transfers population completely from the ground state to the target state. An alternative interpretation is that the resonant field that connects that intermediate and target state dresses the system so that the other laser field can directly transfer population into the dressed state that correlates with the target state. Bergmann and co-workers[62] present a detailed introduction to this type of control strategy, and the reader is directed there for further information.

One of the most recent developments within the field of laser-based control has been the use of intense femtosecond laser pulses in conjunction with adaptive feedback-learning algorithms to optimize the yield of specific photoproduct channels.[8,63,64] This approach exploits the large coherent bandwidth and very high field intensities intrinsic to such pulses and has been successfully demonstrated in the fragmentation−ionization of polyatomic molecules.[9,10] One challenge with the strong field approach is that numerous, simultaneously occurring processes are potentially responsible for contributing to the observed final outcome.[5] These potentially include high-order multiphoton ionization, enhanced ionization,[65,66] nonadiabatic multielectron ionization,[67] and Coulomb explosion,[68] multiphoton resonances leading to propagation on multiple potential energy surfaces, dynamic Stark effects, adiabatic passage by light-induced potentials,[69−71] and bond hardening/softening.[2,72−76] In molecular systems in particular, the theory describing these individual effects is not always well-quantified, and therefore, the challenge of modeling (or understanding in detail) a situation where all of these processes may contribute to the system dynamics is often insurmountable.

Control Interaction

A compelling approach for addressing all of the challenges outlined in the previous sections is the second-order nonresonant dynamic Stark effect (NRDSE). This is a universal interaction that is easily applied with modern laser technology. It exploits the response of a quantum system to the intensity envelope of a laser pulse rather than the oscillating electric field, that is, the effect is highly independent of the spectral content (optical frequencies) of the pulse. The second-order NRDSE operates via a polarizability interaction (often also referred to as a Raman interaction). In special cases, the linear nonresonant dynamic Stark effect may also be applied to the quantum control of molecular systems but requires dipole-allowed transitions between the controlled states.[77] Because all systems containing electrons are inherently polarizable to some degree, the NRDSE approach to control may therefore, in principle, always be applicable and is the focus of the remainder of our discussion. The NRDSE approach requires limited a priori spectral knowledge of the system (Hamiltonian) under consideration because the only important issue in this regard is that the laser field is nonresonant with respect to any real transitions.

In previous publications, we have successfully demonstrated the use of the NRDSE as a tool for the control of molecular axis alignment[78,79] and in the control of chemical branching ratios.[80,81] It should be stressed here that these two effects are identical in terms of the physical control mechanism; they simply act upon different degrees of freedom within the molecular system in question (rotations and vibrations, respectively). More recently, we have also used the Stark effect for transferring population in atomic gas ensembles.[82] In the following sections, we shall explore this assertion in more detail.

DC Stark Effect

The static, or DC Stark, effect is a well-known physical phenomena that was first reported by Johannes Stark in 1914.[83] In the presence of homogeneous electric fields, atomic spectral lines are observed to split into multiple components due to the applied field "mixing" quantum states of different orbital angular momentum quantum number, l. This is analogous to the Zeeman effect,[84] discovered several years earlier in 1897, that is induced by a magnetic field and lifts the degeneracy of states with different magnetic quantum numbers, m_l. The magnitude of the observed Stark effect splitting may exhibit a linear dependence with applied electric field strength for degenerate l states or, much weaker, quadratic dependence for nondegenerate l states. Formally, the general Hamiltonian for an atomic or molecular system in the presence of a static homogeneous electric field may be written as follows

$$H = H_0 + V \tag{2}$$

where H_0 is the field-free Hamiltonian with corresponding eigenstates ψ_n and energy levels E_n. Within the electric dipole approximation, the interaction term, V, between the molecule and the laser field takes the form

$$V = -\boldsymbol{\mu}\cdot\mathbf{E} \tag{3}$$

where $\boldsymbol{\mu}$ is the dipole moment operator and $\mathbf{E}$ is the function associated with the constant linear electric field. At the simplest level of interpretation, we can view the effect of the field as mixing the field-free eigenstates, producing a new distribution of energy levels within the system under investigation, and these new levels may be expressed as linear combinations of the field-free eigenstates

$$\psi^{\text{Field}} = \sum_i a_i \psi_i^{\text{Field-free}} \tag{4}$$

The extent of this mixing is dependent on the strength of the field (a stronger field means more mixing), and this gives rise to the concept of a Stark map that describes the energy levels in a quantum system as a function of field strength. Some good illustrative examples may be found in the work of Goodgame and Softley.[85]

Nonresonant Dynamic Stark Effect

Following eq 1, the semiclassical Hamiltonian for a quantum system in the presence of a time-dependent laser field of frequency ω may be written as

$$H(t) = H_0 + V(t) \tag{5}$$

where

$$V(t) = -\mu E(t) \tag{6}$$

and the linear field $E(t)$ is given by

$$E(t) = e(t)\cos(\omega t) \tag{7}$$

where $e(t)$ is the slowly varying pulse envelope. The derivation of the nonresonant dynamic Stark effect Hamiltonian can be developed from a number of approaches.[79,86] The most expedient approach (which includes the strongest approximations) is to replace the dipole operator $\boldsymbol{\mu}$ with its expectation value, as calculated from its Taylor series expansion

$$\mu(E) = \mu_0 + \alpha E + ... \tag{8}$$

Here, α is the polarizability, which in effect represents an average contribution to the dipole moment from all states not directly participating in the field−system interaction (i.e., those states that are not resonantly dipole coupled by the field, often dubbed "nonessential" states). Dealing with these states in this way greatly simplifies the theoretical treatment of the interaction and leads to the concept of virtual states, which are often invoked in discussions relating to Raman spectroscopy. Following eqs 6−8, we can now rewrite the interaction energy as

$$V = -\int_E \mu(E)\,\mathrm{d}E = -\mu_0 E - \frac{1}{2}\alpha E^2 + ... \tag{9}$$

The field E is oscillating, and the second-order term can be expanded by taking the exponential representation of the cosine function in eq 7.

$$V = -\mu_0 E - \frac{1}{8}\alpha e^2(t)(e^{i\omega t} + e^{-i\omega t})(e^{i\omega t} + e^{-i\omega t}) + ... \tag{10}$$

This is a purely classical approach, but a photon interpretation is already apparent. One photon absorption ($\uparrow$) corresponds to the term $e^{-i\omega t}$, and one photon emission ($\downarrow$) corresponds to the term $e^{i\omega t}$. There are four terms formed from the product of the exponentials. Vertical two photon excitations ($\downarrow\downarrow$,$\uparrow\uparrow$) arise from the terms oscillating at $\pm 2\omega t$. Raman-type excitations ($\uparrow\downarrow$,$\downarrow\uparrow$) arise from the quasi-static terms, which are a product of terms oscillating at ωt and $-\omega t$. Raman transitions can be understood simply by considering that the excitation comprises a photon absorption and a photon emission and therefore depends on frequency differences (and therefore will depend on the pulse envelope) rather than the carrier frequency, ω.

Assuming that the system is unable to respond rapidly, we may develop the dynamic Stark effect potential further. The rotating wave approximation is taken by neglecting the rapidly oscillating (vertical two-photon) terms, which leads to the following

$$V \approx -\mu_0 E(t) - \frac{1}{4}\alpha e^2(t) \tag{11}$$

For the three-dimensional vector case, this is written as

$$V \approx -\mu_0 \cdot \mathbf{E}(t) - \frac{1}{4}\mathbf{e}^*(t)\cdot\alpha\cdot\mathbf{e}(t) \tag{12}$$

where $\mathbf{e}(t)$ is the complex envelope of the field, that is, $\mathbf{E}(t) = \mathscr{R}[\mathbf{e}(t)e^{i\omega t}]$. It is important to note that there are two limiting cases of this interaction, the dipole limit and the Raman limit. In the dipole limit, the interaction follows the instantaneous electric field

$$V_{\mathrm{dipole}} = -\mu_0 \cdot \mathbf{E}(t) \tag{13}$$

However, in the Raman limit, the interaction only follows the pulse envelope squared

$$V_{\mathrm{Raman}} = -\frac{1}{4}\mathbf{e}^*(t)\cdot\alpha\cdot\mathbf{e}(t) \tag{14}$$

Which limit is applicable depends on the system matrix elements (i.e., selection rules) and the extent of any optical detunings (i.e., whether the field frequency is resonant with any real transitions in the system). Here, we are concerned exclusively with the Raman interaction. This choice gives the advantage of having extremely strong interactions due to the immense field strength of ultrafast pulses and yet is independent of the optical frequency (i.e., off-resonance) and therefore not atom- or molecule-specific. As an example, a system with a polarizability of $\alpha = 10$ Å^3 receives a 0.01 eV shift in a 7×10^{11} W/cm^2 field, easily accessible with modern ultrafast laser systems. As we will see later, although seemingly small, shifts of this magnitude can have a profound effect on the dynamics in such systems. The Raman interaction also benefits from the fact that the pulse envelopes (10−1000 fs) are conveniently on the time scale of dynamic molecular processes. Furthermore, we may readily exert a significant degree of control over the form of the envelope itself.

Applications: Molecular Alignment. Experiments designed to interrogate molecular dynamics often employ laser-based methods in order to probe reactant and/or product species. The polarization direction of the laser field therefore serves as a natural frame of reference if one is to make high-order differential measurements that seek to correlate various vector properties present in the products and/or reactants of a chemical process. Examples of such measurements include photoelectron angular distributions in ionization experiments[32,87] and studies of product angular momentum polarization in photofragmentation studies.[25,29] One inherent drawback is that the laser polarization is always defined within the laboratory or space-fixed frame. However, the $\boldsymbol{\mu}\cdot\mathbf{E}$ interaction between the molecular dipole moment and the laser field takes place in the molecular frame of reference. As such, differential measurements made in the lab frame may be "smeared out" or averaged over all possible degrees of molecular frame alignment and/or orientation. Key dynamical information is therefore often obscured. A useful analogy in this regard is the difference between single-crystal and powder X-ray diffraction, the former yielding far greater structural details. In order to alleviate this problem and reveal deeper mechanistic insight into dynamical processes, it is clearly desirable to develop experimental methods that make the lab- and molecule-fixed frames of reference commensurate. This is illustrated, for example, in the case of our time-resolved work on the nitric oxide dimer, where photoelectron angular distributions recorded in the molecular frame of reference using coincidence detection techniques display a far richer structure than those recorded in the lab frame.[38]

In many dynamics experiments, one is dealing with the preparation of excited electronic states, and it is well-known that the optical preparation of such states via resonant absorption will generate a degree of residual alignment in the sample under study via the $\boldsymbol{\mu}\cdot\mathbf{E}$ interaction. This clearly goes some way toward bringing the lab and molecular frames together and does so in a way that is easily quantified (in terms of the relative, anisotropic populations of M_J rotational sublevels) on the basis of well-established angular momentum coupling theory.[88,89] However, this approach is clearly not applicable in instances where one wishes to work with isotropically aligned samples of ground-state molecules. Driven by this limitation, more general methods for inducing alignment using intense laser fields have begun to be developed. In addition, and as will be illustrated further shortly, these nonresonant methods may also be used in conjunction with the preparation of excited electronic states to further enhance the alignment present in these cases, considerably improving the degree of overlap between the molecular and lab frames in order to enhance the differential nature of many dynamics experiments.

Before proceeding further, it is important to make certain terms and definitions clear. From a quantum mechanical perspective, molecular alignment refers to a nonuniform, or anisoptropic, distribution of magnetic sublevels, M_J, in a given angular momentum state (which in a molecular system may contain contributions from electronic and spin components, as well as the angular momentum associated with the rotation of the nuclear framework). Because alignment is quantified by the second moment of the M_J state distribution, there is no difference in population between states with specific $+M_J$ and $-M_J$ values. In the case of orientation, however, which is described by the first moment of the M_J state distribution, specific $+M_J$ and $-M_J$ states may now contain different populations. This is sometimes referred to as a preference for up versus down, but one must be careful in this regard as it is possible to generate an oriented distribution of angular momentum vectors (for example, through the absorption of circularly polarized light) that produces only an aligned distribution of molecular axes.

It is often convenient to characterize alignment in terms of an angle, θ, between an axis that is well-defined in the molecular frame and one that is well-defined in the lab frame. Generally, these are taken to be the principal symmetry axis of the molecule and the polarization direction of the laser light with which that molecule is interacting. Within the photodissociation dynamics community, alignment is generally quantified in terms of an anisotropy parameter, β.[90,91] For the case of a single-photon electric dipole interaction, this gives the following well-known expression for the photofragment angular distribution

$$I(\theta) \propto 1 + \beta P_2(\cos\theta) \tag{15}$$

Here, the $P_2(\cos\theta)$ term is the second Legendre polynomial

$$P_2(\cos\theta) = \frac{1}{2}(3\cos^2\theta - 1) \tag{16}$$

and β is an anisotropy parameter, which is defined as an average over the distribution of angles χ between the axis of the transition dipole moment μ and a photofragment velocity vector.

$$\beta = 2\langle P_2(\cos\chi)\rangle \tag{17}$$

As χ decreases from $\pi/2$ to 0, β increases from -1 (a perpendicular transition) to 2 (a parallel transition), with a value of $\beta = 0$ denoting an isotropic distribution. In the case of prompt (i.e., axial recoil limited) dissociation of a single electronic state of a linear molecule, β is directly related to the distribution of molecular axes prior to dissociation. In the dissociation of more complex systems, there may be a number of electronic states participating in the dynamics, and in general, not all of these will exhibit linear geometries. A single value for β is still observed, and this arises as a result of the averaging of the recoil direction over the lab frame transition moment. With a little more effort on the part of the experimenter, however, the distribution of a molecular axis relative to the transition moment may still be inferred from the β value that is obtained.

Within the strong-field alignment community, two different measures are typically used to quantify the average distribution of molecular axes. The first is the expectation value $\langle\cos^2\theta\rangle$. From eq 16, it can be seen that now we have a situation where $\langle\cos^2\theta\rangle = 1/3$ defines an isotropic distribution, $\langle\cos^2\theta\rangle = 1$ defines maximum alignment (all molecular axes parallel to laser polarization), and $\langle\cos^2\theta\rangle = 0$ represents maximum antialignment (where all molecular axes are perpendicular to the laser polarization direction). Clearly, if one is to use strong field alignment techniques to enhance dynamical observation, it is important that a quantitative measure of the induced alignment be obtained. Typically, this can be achieved, for example, using Coulomb explosion methods in conjunction with 2D fragment imaging.[92,93] This leads naturally to a second way of quantifying alignment, which is to specify the expectation value $\langle\cos^2\vartheta\rangle$, where ϑ (sometimes also denoted as θ_{2D}) is defined as the angle between the laser polarization axis and the projection of the molecular alignment axis (or, more specifically, the projection of the velocity vector associated with a recoiling ion fragment following rapid Coulomb explosion of the molecule) onto the imaging plane. Within this coordinate system, $\langle\cos^2\vartheta\rangle$ takes values of 1 and 0 for the cases of maximum alignment and antialignment, respectively; however, an isotropic distribution now gives rise to $\langle\cos^2\vartheta\rangle = 0.5$.[94]

Generation of rotational axis alignment through the application of infrared laser pulses broadly falls into three categories, (i) adiabatic alignment, where the electric field duration is significantly longer than the period of molecular rotation, (ii) dynamic, impulsive, or "kicked" alignment, for which the field duration is shorter than the rotational time scale, and (iii) the sudden truncation of an adiabatic pulse leading to the projection of an adiabatically evolving state back onto the field-free molecular eigenstates (the so-called switched wavepacket approach). Very recently, a fourth approach using stimulated Raman emission was investigated, which will also be discussed briefly below.

The first detailed theoretical treatments of adiabatic alignment were developed by Freidrich and Herschbach[95] and Seidemann.[96] In applying the NRDSE approach outlined earlier to the specific problem of rotational quantum states, we consider first the case of a diatomic rotor. Within the rigid rotor approximation, the field-free Hamiltonian is given by the expression $H_0 = \mathbf{J}^2/2I$, where $\mathbf{J}^2$ is the squared angular momentum operator and I is the moment of inertia. The eigenstates of H_0 are the spherical harmonic functions, $Y_{J\,M_J}(\theta,\phi)$, and the associated energy levels are given by $BJ(J+1)$, where B is the rotational constant and J is the rotational quantum number. Importantly, under field-free conditions, the rotational Hamiltonian contains no potential energy term, and therefore, the molecule rotates freely in space. Upon application of a slowly varying, intense nonresonant (i.e.,

Raman coupling limit) laser field, as described in the previous section, the time-dependent Hamiltonian now takes the form

$$H(t) = H_0 + V_{\text{Raman}} = \frac{\mathbf{J}^2}{2I} - \frac{1}{4}\mathbf{e}^*(t)\cdot\alpha\cdot\mathbf{e}(t) \qquad (18)$$

For a linearly polarized laser field, the Raman term in the above expression may now be averaged over one optical period to give the following

$$V_{\text{Raman}}(\theta) = -\frac{1}{4}e^2(\Delta\alpha\cos^2\theta + \alpha_\perp) \qquad (19)$$

where the polarizability anisotropy, $\Delta\alpha = \alpha_{||} - \alpha_\perp$ represents the difference in polarizability along and orthogonal to the symmetry axis. The angle between the symmetry axis and the light polarization defines the angle θ. The $V_{\text{Raman}}(\theta)$ term in eq 19 gives rise to a potential minimum along the axis of laser field polarization, as experienced by the molecular axis with greatest polarizability. From a classical point of view, this field-induced potential forces the molecule to librate over a limited angular range, and the new eigenstates of the molecule in the field may be described as a linear combination of the field-free eigenstates.

$$|JM_J\rangle = \sum_J a_{JM_J} Y_{JM_J}(\theta,\phi) \qquad (20)$$

These so-called "pendular" states will experience increased angular confinement as the field strength is increased. In addition, the more polarizable a given molecular system (in terms of the parameter $\Delta\alpha$), the greater the induced alignment because the $V_{\text{Raman}}(\theta)$ potential well is deeper. Experimentally, the adiabatic approach to alignment has been demonstrated for a number of different molecules.[97] The high degree of control over molecular axis alignment that the method imparts is clearly a powerful tool for yielding enhanced differential measurements in certain types of dynamics experiments, for example, photodissociation. However, it may not be suitable for use in other types of experiments where the observable parameters will be influenced significantly by the presence of the externally applied laser field. Obvious examples of this are spectroscopy and diffraction. It is therefore desirable to generate the alignment under field-free conditions, and dynamic methods offer a route to achieving this goal.

Theoretical treatments of dynamical (or nonadiabatic) alignment were first developed by Seideman[96] and Ortigoso et al.[98] for the case of near-resonant and completely nonresonant laser fields, respectively. The concept was first demonstrated experimentally by Rosca-Pruna and Vrakking in the I_2 molecule,[99] and the approach involves the use of an intense laser field that is of very short temporal duration compared to the time scale of molecular rotation. From a quantum mechanical perspective, the dynamical interaction between the molecule and the short, intense pulse induces a series of Raman transitions that effectively result in a rapid "ladder climbing" process that transfers rotational population from lower to higher J states. The results of a calculation illustrating this population transfer for typical experimental field intensities and pulse durations is shown in Figure 1 for the *tert*-butyliodide molecule at a molecular beam temperature of 1 K. As a consequence of this interaction, a large coherent superposition of high-J rotational

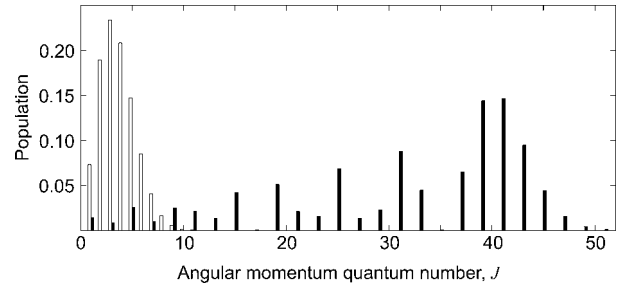

Figure 1. Open bars: relative population of the initial states of *tert*-butyliodide at a temperature of 1 K. Only the populations (including M_J degeneracy) in the $K = 0$ subset of states is shown. Full bars: relative population among the J states in the wave packet excited from the $|JKM_J\rangle = |000\rangle$ initial state by a laser pulse with an intensity of 6×10^{12} W/cm^2 and a temporal duration of 1 ps. The figure is adapted from Bisgaard, C. Z. Ph.D. Thesis, University of Aarhus, 2006.

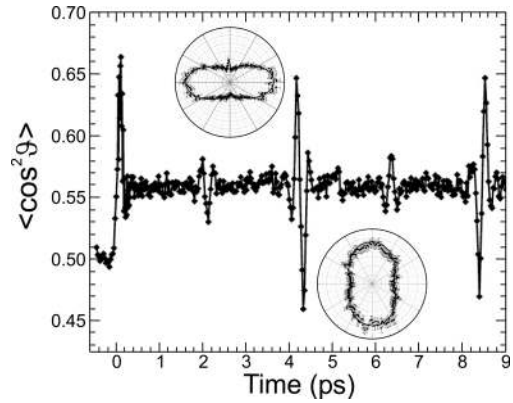

Figure 2. Time dependence of the molecular alignment parameter $\langle\cos^2\vartheta\rangle$ in the N_2 molecule following interaction with a 40 fs laser pulse with a peak intensity of 5×10^{13} W/cm^2. For the half revival at around 8 ps, the maximally aligned and antialigned distributions of molecular axes, obtained using Coulomb explosion imaging, are shown inset as polar plots. This figure is adapted (with permission) from ref 102.

states is generated. The large uncertainty in the wavepacket angular momentum therefore means that a very high degree of confinement in the angular position becomes possible through the angular form of the uncertainty principle,[100,101] and the molecule is therefore highly aligned in the lab frame. The initially prepared wavepacket will then subsequently begin to evolve, initially dephasing but then experiencing revivals at periodically reoccurring times. Critically, these revivals will take place after the short kick pulse is over, and subsequent alignment is therefore generated under field-free conditions. Wavepacket manifolds of high-J states may be generated from any given low-J rotational state present in the sample prior to the application of the aligning pulse, but because there is no coherence between the low-J states in the initial thermal Boltzmann distribution, there is no coherence between the various wavepackets produced. This serves to significantly reduce the overall alignment produced in the sample due to thermal averaging effects. However, this issue may be overcome to a large extent by using molecular beam methods to generate as cold a beam as possible in order to reduce the spread in the initial J state distribution in the sample under study.

An example, adapted from the work of Corkum and coworkers,[102] is presented in Figure 2, showing the revivals obtained in the N_2 molecule using a 40 fs pulse with a peak intensity of 5×10^{13} W/cm^2. The key features of this figure are the initial lab frame alignment ($\langle\cos^2\vartheta\rangle \approx 0.67$) generated during the application of the aligning pulse and the subsequent

field-free return to this value at multiples of 4.15 ps. The initial field-free alignment corresponds to a half-revival of the initially prepared rotational wavepacket and corresponds to a time of $1/(4B)$, where B is the rotational constant of the system under study. The 1/4, 3/4, and full revivals are also observed, and additional subsequent revivals also persist for many tens of picoseconds beyond the range of time delays plotted. It should also be noted that the alignment in between the revival structures does not return to a fully isotropic value (i.e., $\langle\cos^2\vartheta\rangle = 0.5$), as clearly evidenced by the height of the baseline before and after the initial aligning kick pulse is applied. This is a consequence of the $\Delta M_J = 0$ selection rules associated with the ladder climbing process (for the case of a linearly polarized pulse), giving rise to a residual nonstatistical distribution in the M_J sublevels of the high-J rotational states that are prepared. This alignment persists on the typical time scales of the experiment but will ultimately decay due to collisional processes. Each revival producing maximal alignment is also followed shortly afterward by a minimum value of $\langle\cos^2\vartheta\rangle$, which corresponds to maximal antialignment (internuclear axis perpendicular to the laser field). The distributions of molecular axes, obtained directly by Coulomb exploding the N_2 molecules, are included as polar plots in Figure 2 for the first onset of maximal alignment and antialignment.

The degree of alignment produced in experiments of this type may be further enhanced through the use of multiple kick pulses, precisely timed to arrive during full revivals of the initially prepared wavepacket.[103−107] This generates an even broader superposition of coherently prepared rotational states and hence leads to even greater angular confinement. Strategies involving multiple short pulses have also been proposed and demonstrated to reduce the coherent nature of the wavepacket and effectively "switch off" the field-free revivals in the alignment.[108−111] Recently, Suzuki et al. have also demonstrated the use of pulse shaping in conjunction with feedback algorithms to optimize alignment.[112]

The dynamic alignment approach leads to a high degree of angular confinement in the lab frame at periodically recurring times after the laser pulse is over, that is, the lab and molecular frames of reference become very strongly overlapped under field-free conditions. In addition, these revivals may, in many cases, persist for a duration that exceeds the time scale of many dynamical processes. This gives rise to a window in which one is able to perform experiments on highly aligned molecular systems, offering an improved (i.e., more differential) measurement compared to that of an unaligned sample. A recent example is the case of nonadiabatic dynamics and subsequent dissociation in the CS_2 molecule,[113] where pump−probe time-resolved photoelectron spectroscopy (TRPES)[32,87] was used in conjunction with single-particle counting-imaging[36,38] to observe the decay of the initially prepared $^1\Sigma_u^+$ state in CS_2 at an excitation wavelength of 201 nm. The initial geometry of this state is linear, but as the molecule bends (and descends to $^1B_2$ symmetry), it is able to predissociate into $CS(X^1\Sigma^+) + S(^1D_2)$ fragments. Spin−orbit coupling also mediates dissociation into $CS(X^1\Sigma^+) + S(^3P_J)$ fragments. These multiple dissociation pathways evolve over different electronic potential energy surfaces, and a detailed summary of the numerous dynamical investigations of this system undertaken to date may be found elsewhere.[114] The evolution of the photoelectron angular distribution resulting from ionization of the initially prepared excited state of the CS_2 molecule as it begins to dissociate is expected to provide a sensitive probe of the complex system dynamics. However, as shown in Figure 3, the photoelectron angular distributions

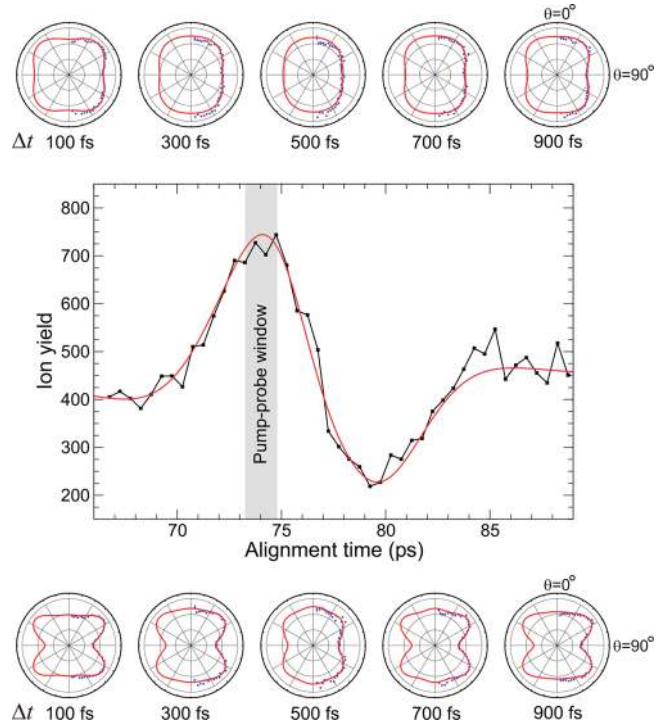

Figure 3. (Top) Polar plots showing photoelectron angular distributions at five different pump−probe time delays, Δt, for an initially unaligned sample of CS_2 molecules. (Middle) CS_2 molecules are transiently aligned by using a short (100 fs), nonresonant (805 nm) laser pulse to create a rotational wavepacket. The alignment dynamics around the half revival are monitored via the two-photon ionization yield (data points). To quantitatively estimate the degree of alignment, we simulated the ion yield as a function of delay using a direct integration of the time-dependent Schrödinger equation to propagate the rotational wavepacket (solid line). (Bottom) The photoelectron angular distributions now obtained at five different pump−probe time delays for the prealigned CS_2 molecules. See main text for discussion.

(PADs) obtained in the lab frame for ionization into the vibrational ground state of the CS_2^+ cation at a series of pump−probe time delays only exhibit these dynamical signatures very weakly due to the alignment averaging effects inherently present with this type of measurement. This is in spite of the fact that the pump step does generate some degree of residual lab frame alignment in the initially prepared $^1\Sigma_u^+$ state ($\langle\cos^2\theta\rangle = 0.55$) through the $\boldsymbol{\mu}\cdot\mathbf{E}$ interaction.

The application of a short (100 fs), intense (4×10^{12} W/cm^2) nonresonant, 805 nm pulse was then incorporated into the experimental setup in order to enhance the degree of overlap between the lab and molecular frames. A significant degree of field-free excited-state alignment ($\langle\cos^2\theta\rangle = 0.74$), which persisted for ∼4 ps, was generated in the system, as shown in the middle section of Figure 3. Critically, this is significantly longer than the dissociation lifetime (<1 ps). By now timing the application of the 201 nm pump pulse to coincide with the full onset of this revival, the differential sensitivity of the probe ionization step (268 nm) is considerably improved. This may be clearly seen in the lower portion of Figure 3, where the associated PADs now display increased anisotropy and a greater angular variation as a function of pump−probe delay. At 100 and 900 fs, the PADs exhibit a local minimum along the molecular frame axis, whereas at 500 fs, there is a maximum in the photoelectron intensity along this direction. This may be attributed to changes in the electronic character of the molecular orbital from which the photoelectron is ejected. There is an optically dark $^1\Pi_g^+$ state which lies at slightly higher energy

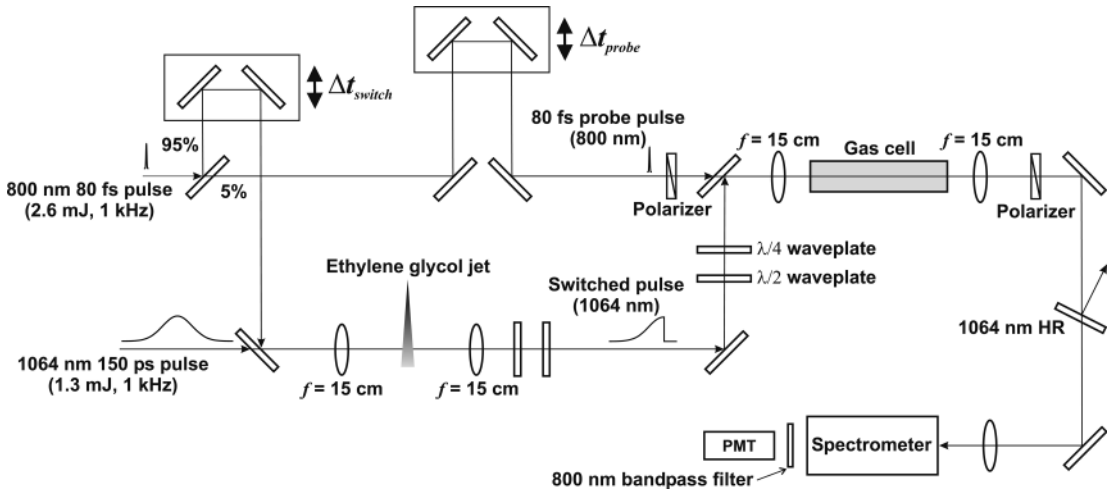

Figure 4. Schematic of the experimental setup used in a switched wave packet experiment. An ethylene glycol jet is used in conjunction with an intense fs laser pulse to create a plasma shutter that produces a "switched" alignment pulse with a rise time of 150 ps and a fall time of 170 fs. This is then used to generate periodically recurring, field-free macroscopic alignment in a cell containing a gaseous sample. The induced alignment is probed by making use of the optical Kerr effect, as described in the main text.

than the initially linear $^1\Sigma_u^+$ state. In a linear geometry, these two states do not interact. However, as the molecule bends, the Renner−Teller effect splits the $^1\Pi_g^+$ state into two components of $^1A_2$ and $^1B_2$ character, the latter of which is now able to interact strongly with the initially excited state. The electronic orbital character of the excited-state wave function therefore evolves as the geometry of the molecule changes; the initially prepared state is predominantly of π^* character, with state mixing (via the Renner−Teller interaction) introducing a σ^* orbital contribution that increases as the geometry becomes increasingly nonlinear. This evolution of the orbital angular momentum character of the excited state is reflected in changes in the l wave composition of the PADs upon ionization at pump−probe delay times between 100 and 500 fs. The fact that the PADs at 900 fs display similar anisotropy to that observed at 100 fs may be attributed to a quantum beat phenomenon which results from the coherent preparation of two distinct vibrational states supported by the linear $^1\Sigma_u^+$ state potential. In future studies employing coincidence imaging methods, we hope to explore the dynamics of CS_2 photodissociation at an even greater level of detail.

In addition to the enhancement of dynamical observations, kicked alignment methods have also been successfully employed as a tool to enhance high-harmonic generation within the rapidly growing field of attosecond science,[115−117] as well as for novel applications such as orbital tomography,[118] a possible route to isotope[110] and spin isomer[119] separation, the optical centrifuge,[120−122] and transient grating spectroscopy.[123−125]

A third approach to the generation of alignment, known as the switched wavepacket (SWP) method, is effectively a hybrid of the adiabatic and kicked approaches. This strategy utilizes an intense laser field that undergoes a slow (adiabatic) rise to generate alignment, followed by a rapid (diabatic) switch-off that induces subsequent rotational revivals under field-free conditions. Experimentally, we have demonstrated the switched wavepacket approach in the alignment of the linear molecules CO_2 and CS_2 and the symmetric top molecule allene (1,2 propadiene).[78,79] More recently, the SWP concept has also been employed by Sakai and co-workers in orientation studies on OCS.[126] The setup for realizing this approach (summarized graphically in Figure 4) utilizes a liquid jet plasma shutter to rapidly truncate a slowly rising laser pulse that generates an initial adiabatic alignment in a molecular sample, as discussed previously. This is achieved by copropagating a picosecond Nd:YAG laser pulse at 1064 nm (the aligning pulse) with a much shorter, high-intensity 800 nm Ti:sapphire pulse of 150 fs temporal duration (the truncation or shutter pulse). Both beams are focused onto the liquid jet (ethylene glycol) with the femtosecond pulse timed to arrive just as the aligning pulse reaches maximum intensity. The relatively low intensity ($\sim 10^{11}$ W/cm^2) of the aligning pulse allows it to pass through the jet unmodified; however, the intensity of the truncation pulse ($\sim 10^{13}$ W/cm^2) is sufficient to cause dielectric breakdown of the ethylene glycol and generates a plasma which effectively serves to rapidly switch off the trailing part of the aligning pulse, suddenly projecting the field-dressed eigenstates of the molecule back onto the field-free basis set. This results in a coherently prepared wavepacket of rotational states that will dephase and then subsequently exhibit rotational revivals under field-free conditions in a manner similar to that in the kicked alignment process.

The experiments were carried out in a room-temperature gas cell, into which the rapidly truncated aligning pulse was focused. The gas cell was positioned between a pair of Glan−Taylor polarizers oriented at 90° with respect to each other (and at 45° to the alignment pulse). The overall setup is included in Figure 4. The detection of the alignment generated in the molecular sample contained within the cell was then determined by propagating an additional (probe) laser pulse (800 nm) through the cell plus polarizer arrangement. In the absence of the aligning pulse, transmission of the linearly polarized probe through the experimental setup onto a photomultiplier (via a monochromator) is completely extinguished at the second polarizer. In the presence of the aligning pulse, however, a degree of lab frame axis alignment is produced in the sample contained within the cell. This induces macroscopic birefringence within the sample, and the probe beam polarization will therefore experience an optical rotation (the optical Kerr effect), the extent of which will be dependent upon the degree and direction of the sample alignment.[79,127] The probe pulse will therefore now propagate through the second polarizer to some extent, and a nonzero signal will be detected at the photomultipler. By monitoring this signal as a function of the delay between the truncation pulse and the probe pulse, the evolution of the field-free revivals in the sample alignment may be monitored, as illustrated in Figure 5 for the case of CO_2. Key features of note in Figure 5

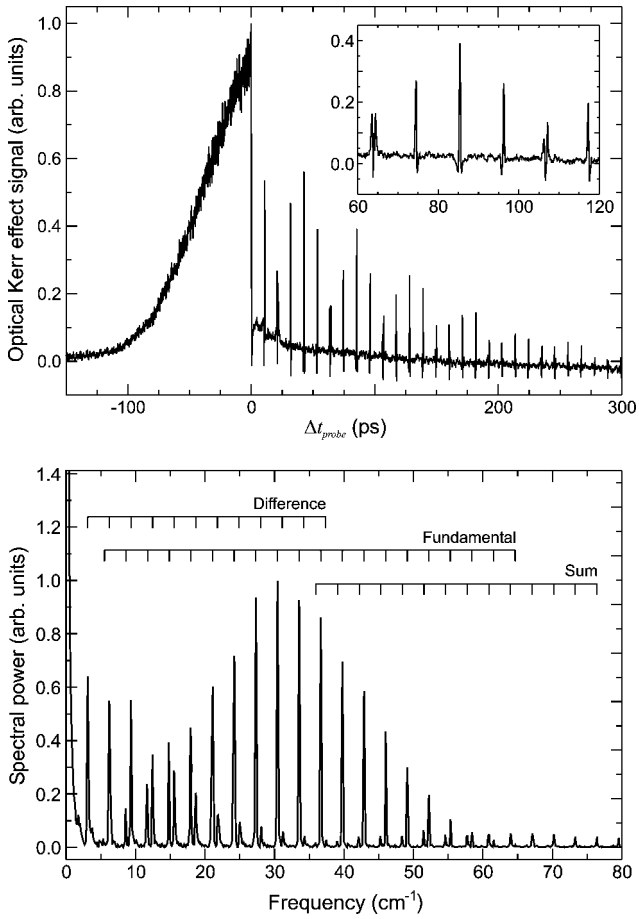

Figure 5. (Top) Switched wavepacket optical Kerr effect signal from CO_2 as a function of probe delay time at 300 Torr and 300 K. At $\Delta t < 0$, the probe monitors the adiabatic alignment generated by the slowly rising edge of the aligning pulse. At $\Delta t > 0$, the aligning pulse has been rapidly truncated, and field-free wavepacket revivals are seen with a spacing of 10.7 ps $=1/8B$. (Bottom) Fourier transform of the optical Kerr effect signal from CO_2 at 300 Torr and 300 K. Combs indicating progressions of lines corresponding to the fundamental, difference, and sum frequencies are shown. Each progression consists of lines with a measured spacing corresponding to $8B$, with $B = 0.39$ cm^{-1}.

are the steady overall decrease in revival intensity with time (a consequence of collisional decoherence in the cell) and the spacing of the revival peaks, which occur at $1/(8B)$ rather than $1/(4B)$ as a consequence of the nuclear spin statistics in CO_2 giving rise to odd J-levels with zero statistical weight. The observed spacing in the revivals of 10.7 ps therefore corresponds to a value of $B = 0.39$ cm^{-1}, in agreement with values reported from conventional spectroscopic measurements.[128] Upon closer inspection, the intensities of the revival peaks also show a marked fluctuation from one revival to the next, and a pattern of intensities appears to repeat periodically. Because the revival structure reflects the field-free energy level spacing of the system under study, the origin of this behavior becomes more apparent upon taking the Fourier transform of the evolving optical Kerr effect signal versus time. This is also shown in Figure 5, and three distinct progressions of lines, all exhibiting the same line spacing but offset with respect to each other, are now clearly seen. These progressions correspond to the fundamental, sum, and difference frequencies associated with the allowed transitions in CO_2, and a detailed discussion relating to the origin of these features may be found elsewhere.[79]

Compared with microwave spectroscopy, the technique traditionally used to perform rotational spectroscopy of ground-state molecules, the field-free alignment approaches demonstrated here have a number of appealing benefits; there is no requirement to tune either the aligning pulse or the probe pulse into resonance with the rotational transitions, no permanent dipole moment is required in the molecule under investigation, and no Doppler broadening is present.

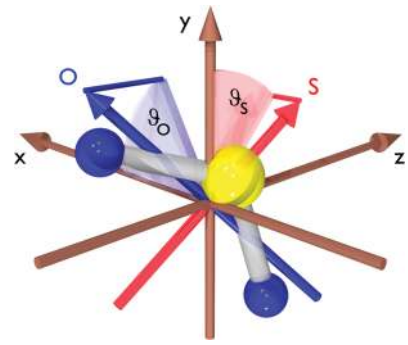

Figure 6. Definition of angles ϑ_O and ϑ_S. The laboratory frame is defined by the polarization direction of the two laser pulses (the z-axis) and the polarization directions of the two linearly polarized alignment pulses; the first pulse is polarized along the x-axis and the second along the y-axis.

All three of the approaches to generating molecular alignment outlined above clearly open up exciting new possibilities for enhancing the differential nature of experiments that seek to probe the complex dynamical processes that take place in molecular systems. However, one inherent limitation of these approaches is that the alignment generated is restricted to a single axis within the molecular system under study (the axis that exhibits the greatest polarizabiltiy). For linear rotors, this one-dimensional alignment is obviously sufficient, but for more complex molecules (symmetric top and asymmetric rotors), there is no alignment generated in the other two axes. However, in many dynamics experiments, this is clearly desirable in order to further enhance the differential nature of any measurement. Initial efforts to address this issue, both from theoretical and experimental standpoints, focused on the use of elliptically polarized pulses to generate three-dimensional alignment, using either the adiabatic[129] or kicked[130−132] approaches. From an adiabatic perspective, one can view the process as the molecule minimizing its energy in the applied laser field by aligning the largest polarizability axis along the major axis of the field and the next largest polarizability axis along the minor axis of the field. Once these two axes are confined to some extent, the third axis must clearly also be confined (along the axis perpendicular to the polarization plane). However, there is a trade off between alignment of the first axis versus that of the second.

An alternative strategy to achieve 3D alignment is the use of multiple pulses with orthogonal polarizations.[133,134] We have successfully demonstrated this approach for the generation of field-free 3D alignment (FF3DA) in the SO_2 molecule.[135] Briefly, we employed an initial 180 fs pulse with a central wavelength of 815 nm and an intensity of 2×10^{13} W/cm^2 to align the most polarizable axis in the system, which in this instance is along the O−O direction, as illustrated in Figure 6. For simplicity, we denote this the O-axis. Critically, the short duration of the aligning pulse means that maximum alignment initially induced in this axis occurs after the pulse is over. Rather than wait for a dephasing and subsequent revival of the alignment of this axis, a second, orthogonally polarized pulse of 50 fs duration (815 nm, 2×10^{13} W/cm^2) was applied only a few hundred femtoseconds later to align the second most polarizable axis (which lies in the plane bisecting the O−S−O

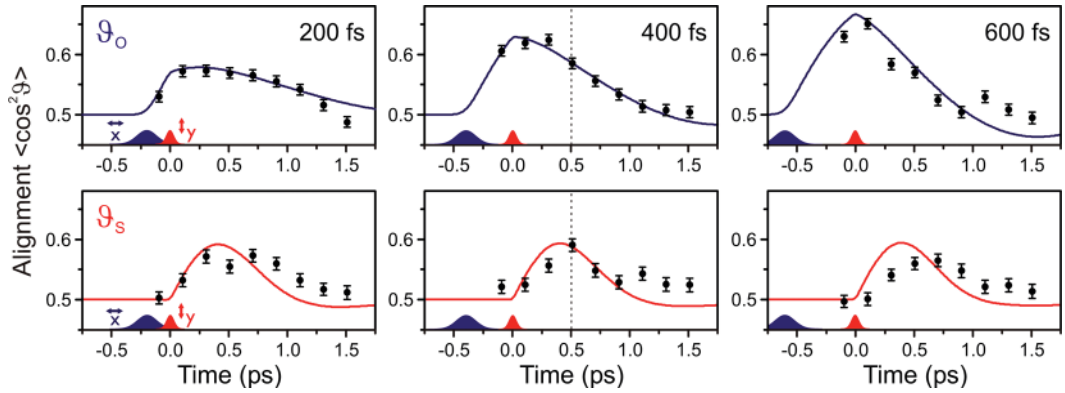

Figure 7. Time dependence of SO_2 molecular axis alignment for three different temporal delays between the two alignment pulses described in the main text. Zero time is defined by the peak of the second alignment pulse. Experimental data points are shown along with the results of classical calculations (solid lines). The dashed line at 400 fs shows the maximum FF3DA achieved.

bond angle and is denoted as the S-axis). A shorter pulse may be used in the second step due to the fact that rotation about the S-axis has a larger moment of inertia than rotation about the O-axis. By carefully adjusting the time delay between the application of the two aligning pulses, a situation where maximal 3D alignment is generated may be found. This was determined directly using multibody coincidence imaging of ion fragments produced following Coulomb explosion of SO_2 using a third time-delayed laser pulse (815 nm, 50 fs, 5×10^{15} W/cm^2). As shown in Figure 7, the optimal delay time for maximum FF3DA in the case of SO_2 was found to be 400 fs. The use of multiple pulses with orthogonal polarizations offers a very flexible and general route to achieving 3D alignment in polyatomic molecules because the duration, intensity, and time separation of the laser fields may be individually tailored to maximize the effect for any specific system of interest.

Recently, a hybrid approach has been developed for the generation and amplification of rotational coherence.[136] This technique simultaneously involves two very different limits of control, weak impulsive control (to exceed the random vacuum fluctuations) and strong pumping via stimulated Raman emission. The approach prepares high-coherence rotational dynamics that are phase-stable with respect to ultrashort pulses. The rotational coherence is made phase-stable with respect to a separate source of ultrashort pulses by weakly seeding the vacuum fluctuations. The rotational amplification is achieved using a phase-independent nanosecond pump pulse to prepare the coherence in molecular hydrogen. The approach can be used to generate large amounts of rotational alignment and has been used to generate spectral broadening of femtosecond pulses.

As a final conclusion to this section, we note that the ability to produce field-free molecular axis orientation in molecular systems offers a route to enhancing the differential nature of dynamics experiments to an even greater extent. Very recently, several groups have made significant experimental progress toward this goal using a combination of intense laser fields in conjunction with static field devices.[126,137,138] This raises many interesting prospects for application of these approaches in future generations of molecular dynamics experiments.

Applications: Photochemical Control. The NRDSE approach also finds application in the area of chemical control, that is, the direct modification of product yields in a chemical reaction. As we stressed earlier, this is achieved through the same basic physical effect, with the only difference now being that it acts on the vibrational rather than rotational degree of freedom in the system under study. There is a long history of studies that have sought to investigate vibrational control using strong laser fields using effects such as bond hardening and softening and adiabatic passage by light-induced potentials in order to mediate dissociation rates and position localization in molecular systems.[2,69−77] A distinction between the various techniques is whether or not the control is derived from resonant dipole interactions or nonresonant Raman interaction. Here, we consider only the use of the nonresonant Raman interaction alone (induced from adiabatically eliminated states) to perform the control. The technical details are outlined above, but for a more detailed discussion of the relation between the two approaches, the reader is directed toward the review by Shore[139] and some of the recent publications by Solá and co-workers.[140−143]

As highlighted previously, there are, in general, a large number of competing high-order, nonlinear effects that may all potentially contribute to the overall system dynamics in the presence of an intense laser field (>10^{13} W/cm^2). In molecular systems in particular, the theory describing these individual effects is not always well-quantified, and therefore, the challenge of modeling a system where all of these processes are contributing to some degree in modifying the dynamics is often insurmountable. Such issues have given rise to the widespread use of feedback-based learning algorithms in order to provide shaped laser pulses that are tailored to achieving a specific product yield in a control experiment. While such approaches benefit from the fact that very little, if indeed any, a priori knowledge of the Hamiltonian for the system under the influence of a strong field is required, in the longer term, this is clearly an undesirable situation if one wishes to learn more about the underlying physics of the control interaction. Because the nonresonant dynamic Stark effect manifests itself as the field intensity is gradually increased, we may study its influence on a molecular system by choosing to work in a field intensity regime that induces Stark shifts of sufficient magnitude to exert an influence over the dynamics yet produces a negligible contribution from other strong field effects, such as multiphoton ionization. Typically, this is a regime on the order of 10^{12} W/cm^2. Additionally, in the first instance, we chose to work only with simple Gaussian pulse shapes. These steps greatly simplify the nature of the control interaction, making it far easier to develop a working model of the physics involved. As we will show, however, the control that can be produced under these conditions is very substantial, both in terms of magnitude and flexibility.

To illustrate the principle of dynamic Stark control (DSC) in regard to photochemical control, we begin by considering an arbitrary diatomic molecular system, AB, with three electronic states, the ground state (state 0) and two electronically excited

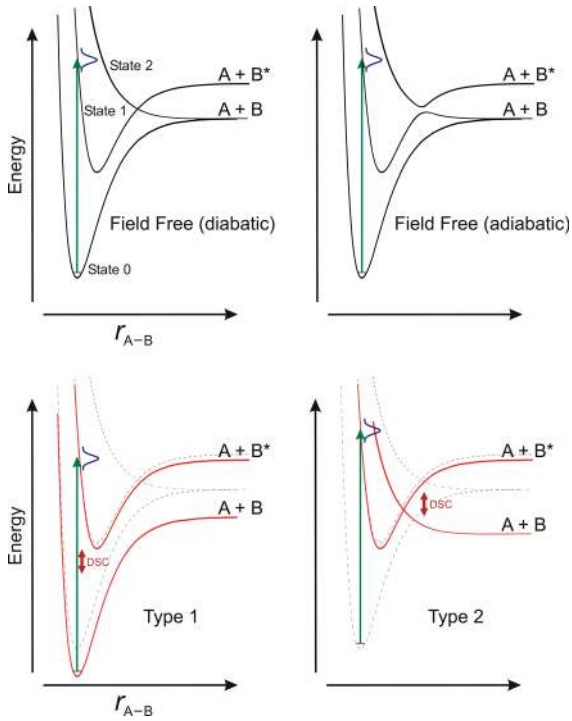

Figure 8. Schematic illustration (with Stark shifts greatly exaggerated) of the DSC approach to chemical control. A full discussion of the process is given in the main text. For clarity, the adiabatic representation of the excited-state potentials is only shown for the field-free case, and only the Stark shifts that are directly relevant to the modification of the dynamics for each of the type 1 and type 2 strategies are shown.

states, one of which is bound (state 1) and one which is purely dissociative (state 2). Diabatically, these two excited states correlate to different (spin−orbit) atomic products in the asymptotic region, A + B* and A + B, respectively. Because B and B* will typically have different chemical reactivity, the asymptotic limits correspond to two distinct chemical product channels. In the event that state 1 and state 2 possess the same symmetry, there is the possibility of an avoided crossing modifying this picture to give new adiabatic states. The overall scheme is shown in Figure 8. Upon electronic excitation, a wavepacket may be prepared on the state 1 potential, and if sufficient energy is absorbed, it will not remain trapped in the bound potential well as it evolves. Within the Born−Oppenheimer approximation, state 1 will then simply dissociate adiabatically to give A + B products exclusively. However, in the event of significant coupling between the electronic and nuclear degrees of freedom in the system (i.e., a breakdown of the BO picture), a crossing onto the state 2 potential curve may take place, ultimately resulting in the production of A + B* products. This nonadiabatic effect gives rise to a natural branching ratio of B/B* products that will typically vary to some extent as a function of excitation energy. In a simple diatomic system such as that under consideration here, the propensity for adiabatic versus nonadiabatic behavior may be described by the Landau−Zener formula[144−146]

$$P = \exp\left[\frac{-2\pi V_{12}^2}{v\partial_R(V_1(R) - V_2(R))}\right] \tag{21}$$

The above expression essentially states that the probability of crossing to state 2 is mediated by three factors, the extent of the coupling between the two states (the V_{12}^2 term in the numerator), the relative slopes of the two potential energy surfaces near the crossing region (the $\partial_R(V_1(R) - V_2(R))$ term in denominator), and the velocity with which the initially prepared wavepacket traverses the crossing point (the velocity, v, in the denominator). Of these, it is the wavepacket velocity that will, at least at the first level of approximation, provide the effective "handle" for the DSC control interaction in this system. To begin with, in very simplistic terms, one can consider the molecular orbitals associated with state 1 and state 2. In the former case, we have a bound electronic state, and as such, there will be significant electron density localized between the two atoms A and B. In the case of the purely dissociative state 2, there will be a node in the electronic distribution in this same region. Owing to the very different electronic geometries exhibited by the two states, it is therefore reasonable to expect the magnitude of the polarizabilities and therefore the Stark shifts exhibited by each state in the presence of a field to be different, that is, the state energies will shift relative to each other. More formally, we can write the relevant Hamiltonian for a given state by expressing eq 5 explicitly in terms of the vibrational coordinate, x

$$H(t) = \frac{p^2}{2\mu} + U(x) + V(t) \tag{22}$$

Here, $U(x)$ is the intramolecular vibrational potential, and we are assuming, as a first approximation, that the interaction term $V(t)$ is coordinate-independent (i.e., the magnitude of the Stark shift for each specific state will effectively be constant for all internuclear distances). By following the same arguments as outlined in eqs 6−14, we arrive at the same answer for the induced Stark potential within the Raman coupling limit

$$V(t) = -\frac{1}{4}e^2(t)\alpha \tag{23}$$

Here, $e^2(t)$ simply is proportional to the field intensity as a function of time. As a consequence of the relative energy shift induced by the different polarizabilities, α, for state 1 and state 2, the position of the point where the potential energy curves for these two states cross will be altered. The excited-state wavepacket initially prepared on the state 1 potential will therefore encounter the crossing with state 2 at a different point along its trajectory toward the asymptotic product limit. Because the velocity with which the wavepacket is traveling at this point is now different from the situation when the control field is not applied, the propensity for diabatic versus adiabatic dissociation will be modified, as expected from the Landau−Zener model. The B/B* branching fraction is therefore also changed (relative to the field-free case). This concept is illustrated graphically in Figure 8 for the case where the crossing moves to a lower point within the state 1 potential well, and the wavepacket velocity at the crossing is therefore increased relative to the field free case. The B* channel in consequently enhanced (more diabatic behavior). A situation where the crossing moves up relative to the field-free case would conversely enhance the yield of ground-state product, B, (more adiabatic behavior) due to a slowing of the wavepacket velocity. Finally, it should be noted that because the nonresonant control field is chosen to be short on the time scale of the overall dissociation event, the system will have returned to its original field-free state before the wavepacket fully reached the asymptotic product limit; hence, although the product branching ratio is altered, the kinetic energy

released into the fragments is unchanged relative to the situation when the control field is not applied, although this depends in a complicated way on the asymptotic properties. For the purposes of discussion later, we will denote this type of control interaction (i.e., one that directly mediates the crossing between different excited states after the initial excitation from the ground state) as type 2.

We now turn our attention to the situation where the control field may be used to modify the initial wavepacket preparation on the state 1 potential, that is, when the control pulse is applied at the same time as the pulse that induces the electronic transition between state 0 and state 1. Just as with the type 2 case already discussed, there will be a relative Stark shift in the energies of the two states, owing tp the different electronic geometries they each exhibit. Although in the example shown in Figure 8 the two states (0 and 1) are both bound, the promotion of an electron to a higher-lying (more loosely bound) molecular orbital will clearly still alter the polarizability of the system to some extent. Inducing a differential Stark shift during the excitation step therefore serves to alter the starting point for the wavepacket trajectory on the state 1 potential by effectively detuning the excitation step to some degree. As illustrated in Figure 8, the wavepacket born on the state 1 potential now begins its trajectory at a lower point, and hence, it encounters the crossing with state 2 with a reduced velocity, enhancing the propensity for adiabatic behavior (and the associated yield of the A + B product channel) relative to the field-free case as a result. We will denote this type of control interaction (i.e., one that influences the wavepacket starting point on the initially prepared excited-state surface) as type 1.

Finally, key points to stress here are that (i) owing to the sensitivity of the crossing, only very small differential Stark shifts (on the order of 0.1 eV or less) are required to induce significant changes in product branching ratios,[80] (ii) the type 1 and type 2 strategies together offer the possibility of bidirectional control over the chemical branching ratio in many systems, and (iii) the control interaction only involves neutral species; in contrast to other control strategies, no ions are formed directly during the control interaction, and in fact, there is no net absorption of photons from the control pulse. Control is exerted only on the potential surfaces of interest (i.e., those that participate directly in the dynamics even in the absence of the control field).

The use of the NRDSE for chemical control has been demonstrated experimentally in the photodissociation of the IBr molecule.[81] Absorption of light in the 520 nm region leads to the formation of IBr in the $B^3\Pi(0^+)$ excited state, which subsequently dissociates into two distinct product channels, $I(^2P_{3/2}) + Br(^2P_{3/2})$ and $I(^2P_{3/2}) + Br^*(^2P_{1/2})$, the latter resulting as a consequence of nonadiabatic coupling to the $Y^3\Sigma^-(0^+)$ state. In the absence of any externally applied control fields, the Br*/Br branching ratio takes a value of around 3:1.[147] There are a number of appealing features about IBr and this specific excitation scheme that make it a good candidate for use in a NRDSE control experiment. (1) The absorption spectroscopy and photodissociation dynamics are already well-characterized with experimentally convenient wavelengths for both the initial excitation and the subsequent detection of photoproducts. (2) The $B^3\Pi(0^+)$ and $Y^3\Sigma^-(0^+)$ states are not expected to be strongly dipole coupled[148] (i.e., the Raman interaction will dominate). (3) The IBr molecule is highly polarizable, meaning that relatively large Stark shifts may be achieved with relatively modest control field intensities ($<10^{13}$ W/cm^2, in this particular instance). (4) The relatively long dissociation lifetime of the IBr excited state (>500 fs) means that the control field may be applied

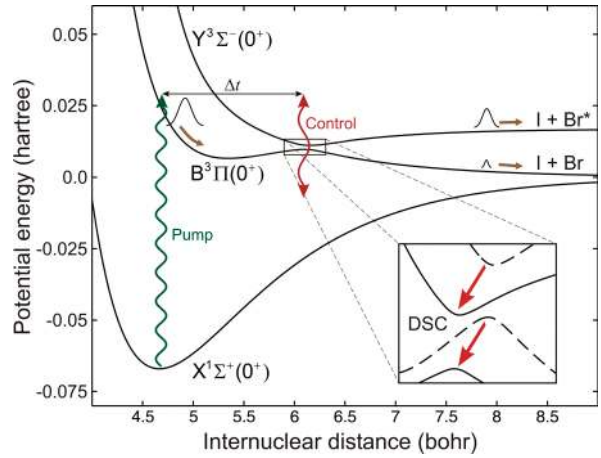

Figure 9. DSC of IBr dissociation. An excited-state wavepacket traverses a nonadiabatic crossing, correlating to either $I + Br(^2P_{3/2})$ or $I + Br^*(^2P_{1/2})$ products. As the IBr molecule dissociates, an ultrafast, nonresonant IR field is used to dynamically modify the adiabatic potential barrier (inset) via the Stark effect, mediating the reaction outcome. Because no transitions to other electronic states are involved, the system always remains on these two coupled potentials.

precisely at various points along the dissociation coordinate using nonresonant IR pulses on the order of 100 fs duration, something easily achieved with modern ultrafast sources.

The overall experimental strategy is summarized in Figure 9. Briefly, preparation of the excited $B^3\Pi(0^+)$ state is accompanied by the application of a nonresonant control field, which may be carefully timed to arrive just before, during, or just after the exciting pump transition. Because the proposed DSC mechanism is mediated by the intensity of the control field rather than its spectral content, it is generally desirable to tune the wavelength of the control pulse to be as red as possible, that is, as deep into the infrared region of the spectrum as one is able to go, in order to maximize the strength of the control field (and hence maximize the potential DSC control effect) before the onset of unwanted multiphoton ionization processes. The only obvious caveat here is that the control field must not become resonant with any vibrational transitions in the system under study.

Following the application of the excitation and control pulses, a third weak-field (probe) pulse was then used to ionize the ground-state ($^2P_{3/2}$) iodine atom fragments formed following photodissociation of the IBr. Because the ground-state iodine atoms are common to both photofrgament product channels that may result at 520 nm, the kinetic energy release distribution of these atoms provides a direct measurement of the relative Br*/Br yield. The probe pulse ionizes the iodine atoms via a (2+1) REMPI scheme,[149] and the resulting I^+ ions are monitored using the technique of velocity map imaging in order to provide full energy and angle-resolved information.[150] The probe pulse is significantly delayed in time with respect to the pump and control pulses (in this case, by 60 ps) in order to ensure that it does not influence the dynamics directly. Owing to the very narrow widths of atomic resonances, it is desirable to use as narrow of a line width as possible for the probe pulse in order to maximize the resonant detection of the atomic fragments produced. In experiments utilizing ultrafast sources, narrow line widths through restricted phase matching may be achieved using long (e.g., ~1 cm) nonlinear crystals for the generation of the required probe wavelengths.

Figure 10 shows the raw iodine recoil speed distributions obtained as a function of the delay time, Δt, between the pump

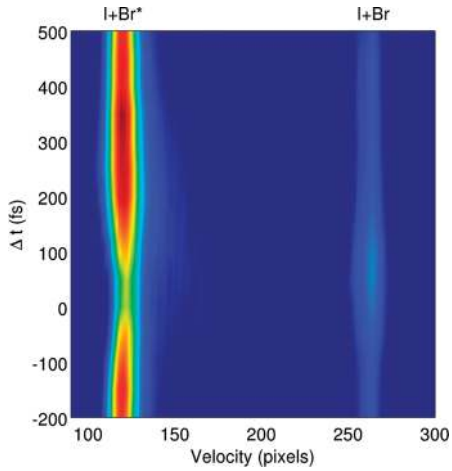

Figure 10. Experimental iodine atom recoil speed distributions showing the relative branching into I + Br and I + Br* product channels in the DSC-mediated photodissociation of IBr as a function of control pulse delay.

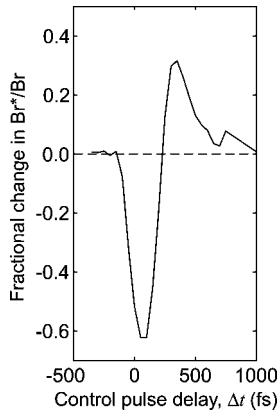

Figure 11. Fractional change in the Br*/Br branching ratio relative to the case when no DSC field is applied. The branching fraction is measured by taking the ratio of the integrated intensities of the two peaks in Figure 11 as a function of Δt, the control pulse time delay. At early and late delays, the field-free branching ratio is observed, demonstrating the reversible nature of the DSC interaction.

and control pulses. There are a number of important points to take from this result. First, application of the control pulse either well before the excitation step takes place ($\Delta t = -200$ fs) or after the dissociation has fully taken place ($\Delta t = +500$ fs) does not alter the product branching ratio from that obtained when the control field is not applied at all (i.e., the Br*/Br yield is ~3:1, the same at that observed previously in "passive" observations of the dynamics[147]). That is, the process is nondestructive. Second, there are two specific time delays when the product branching ratio is critically sensitive to the control field. At around $\Delta t = 0$, there is a clear suppression of the Br* channel with an accompanying enhancement of the Br yield (type 1 control). In addition, at around $\Delta t = +200$ fs, the opposite situation arises, with the Br* channel now being enhanced and the Br channel conversely suppressed (type 2 control). This is a clear indication of the bidirectional nature of the control that is possible with the DSC approach, as discussed previously. Figure 11 shows the fractional change in the Br*/Br branching ratio relative to the situation in which the control field is not applied. A peak to valley contrast of around 90% is observed, and, importantly, because we are operating at field intensities beyond the perturbative limit, this high degree of control is exerted on 100% of the reacting population rather than some small fraction of it. Finally, and perhaps most importantly in the context of demonstrating the exact, reversible nature of the DSC control interaction, the kinetic energy release distribution is unchanged for all Δt values, clearly illustrating that no additional real electronic transitions have been induced, that is, there has been no net absorption of photons during the control interaction, and we have effectively stayed on the same potential surfaces throughout the dissociation event. As such, the DSC method has successfully modified a potential energy landscape using an intense laser field, controlling a photochemical outcome in the process, but without any photons being consumed in the process. In this regard, the DSC approach to chemical control may be viewed as a photonic catalyst, which is in contrast to the photonic reagent methodologies involved in other strong-field control approaches, where the control pulse photons are absorbed in order to transfer population between different real electronic states.

Conclusions and Outlook

We have discussed the notion that in order to fully understand dynamical processes in chemical systems, that is, the evolution of the electrical forces in the system as reactants transform into products, it is generally desirable to make the most differential measurement possible. We have also discussed the idea that the use of externally applied forces may provide strategies for control that can enhance these dynamical observations. The nonresonant dynamic Stark effect, induced by strong laser fields, is a powerful tool for bringing the lab and molecular frames of reference together in order to realize these improved dynamical observations. The nonresonant dynamic Stark effect may also be used to actively modify the outcome of product branching yields in neutral molecule photodissocation. This is achieved through the application of laser fields that are of sufficient intensity to modify potential energy barriers during the dissociation event without themselves inducing further fragmentation of the molecular system under study (i.e., a nonpeturbative but nonionizing, or nondestructive, control strategy). In effect, these fields may be viewed as photonic catalysts rather than photonic reagents. The DSC approach therefore provides an intuitive alternative to some other strong-field quantum control strategies.

In order to further develop the DSC approach to chemical control, we would argue that it is important to begin incorporating more differential experimental approaches, such as have been discussed to some extent earlier in this article. In effect, one goal for the next generation of DSC experiments is to move beyond the product yield measurements that have largely been used in control-based observations up to now in order to gain enhanced insight into the control interaction itself. One example of this is to begin considering how various photoproduct angular momentum vector correlations are changed as a result of the control field interaction. As first demonstrated experimentally by Zare and co-workers[27,151,152] in the ICl molecule, and subsequently expanded upon by a great many researchers looking at a large number of different systems,[29] the polarization of angular momentum in photofragment recoil is a powerful probe of the nonadiabatic interactions that have taken place during a photodissociation event. In particular, observations of electronic angular momentum orientation provide a detailed signature of the phase shift between different coherent pathways connecting the same initial and final states (a matter−wave interference effect). In a DSC experiment, differential Stark shifts clearly have potential to modify such phase shifts significantly during a dissociation event. By making detailed observations of the angular momentum polarization in photof-

ragments produced in a DSC experiment, it is hoped that a far greater understanding of the control interaction may be developed. Employing techniques that probe the vector properties of photofragments will also be of great potential value if one wishes to try and introduce additional control parameters into DSC experiments by using shaped laser pulses. The important caveat here is that, at least in the first instance, it is clearly desirable to modify the DSC control pulse in a highly systematic way. Building the complexity incrementally is paramount in order to begin developing a full understanding of the underlying control from the vector correlations in the resulting photoproducts. In addition to being demanding experiments, this approach will, of course, also present new challenges to theory.

Dynamically induced phase shifts also offer some interesting possibilities when applied to systems that do not dissociate directly. As we have shown theoretically in previous work,[80] DSC may also provide a route to enhancement or reduction of excited-state lifetimes. The scattering wave function at an avoided crossing consists of two different electronic components, corresponding to the two molecular states in question. The application of a short Stark shift will introduce a different energy shift for the two different electronic states. The subsequent accumulation of an anomalous phase difference between the two states can be used to significantly alter the subsequent dynamics. The reason is that a scattering wave function correlates to the same state if a phase is added to both electronic states simultaneously. However, adding a relative phase to one electronic component changes the state to which the wave function is correlated, hence altering the subsequent dynamics. In calculations, this mechanism has been used, for example, to alter the lifetime of states dissociating through an avoided crossing.

Another important step in the development of the DSC approach to chemical control will be its application to larger, more complex systems. As stated previously, because DSC exploits the molecular response to the field intensity rather than its spectral content, limited spectral knowledge of the system under study is required, and the approach should be generally applicable and scalable. In many large molecular systems, multiple conical intersections may be traversed as the initially prepared state evolves toward the final product state distribution, and one can envisage the use of multiple control pulses, each precisely timed, to affect control at several different points along the reaction coordinate.

Ultimately, it is also desirable to apply the DSC approach to liquid-phase systems. This presents several technical challenges, particularly if one wishes to keep striving to understand, in detail, the subtle mechanistic details of the control interaction because many of the highly differential measurements that are a staple of gas-phase chemical dynamics studies are much more challenging, if not impossible, in this type of medium. This situation is further compounded in the case of strong field control as the propagation of intense laser pulses through dense media results in a significant modification of the pulse structure through phenomena such as self-phase modulation and self-focusing. As such, great care must be taken in experiments of this type in order to ensure that the pulses inducing the DSC interaction are properly characterized. In the first instance, these issues may be overcome by using thin liquid jets,[153] and although this approach clearly limits any potential large-scale application, it is an essential first step toward developing a detailed understanding of the underlying control.

Finally, lying at the intersection of control and observation are quantum information, computation, and communication (QICC). QICC research utilizes the intrinsic uncertainty of quantum mechanics, providing fundamental advantages over operations with classical systems. In order to provide these advantages, however, accurate system articulation and observation is required. As the ability to observe and control quantum processes get better, we are offered a more detailed view of the microscopic world. As our understanding is consequently improved, so too is the way that we think about it. Specifically, the interrelated ideas of control and observation can also be augmented with quantum information and computation, which then forms a triad of connected methods: observe, control, and process. As an analogy, the methods appear more and more like our notions of look, touch, and think. The links between quantum control and quantum information are still developing, but there are a number of exciting avenues.

In particular, quantum memories are an essential component of quantum networks.[154] Optical quantum memories store and controllably re-emit photons, preserving their initial quantum characteristics with high efficiency and fidelity. Because memories are actively controlled components that need to be enabled to write and read, they tend to be highly related to control approaches. For example, the high-speed Raman protocol uses the nonresonant Stark shift to sweep an absorption transition during the storage of a photon.[82,155,156] This process dynamically generates bandwidth from a narrow transition, and the increased bandwidth now offers the potential for GHz data rates, a thousand-fold increase over other techniques. The application of the DSC approach in this rapidly growing research area will present many exciting challenges for the future.

Acknowledgment. We thank our co-workers and collaborators who have contributed in a variety of ways to the work that has been highlighted here, C. Bisgaard, O. J. Clarkin, P. B. Corkum, O. Gessner, C. C. Hayden, M. Yu. Ivanov, R. Lausten, A. M. D. Lee, K. F. Lee, J. Mottershead, M. Spanner, J. G. Underwood, D. M. Villeneuve, and G. Wu. We would also like to thank NSERC for funding.

References and Notes

(1) Brumer, P. W.; Shapiro, M. *Principles of the Quantum Control of Molecular Processes*; Wiley-Interscience: Hoboken, NJ, 2003.
(2) *Molecules in Laser Fields*; Bandrauk, A. D., Ed.; Marcel Dekker: New York, 1994.
(3) Gordon, R. J.; Rice, S. A. *Annu. Rev. Phys. Chem.* **1997**, *48*, 601.
(4) Rice, S. A.; Zhao, M. *Optical Control of Molecular Dynamics*; John Wiley and Sons: New York, 2000.
(5) Sheehy, B. *Annu. Rep. Prog. Chem., Sect. C* **2001**, *97*, 383.
(6) Rice, S. A. *Nature* **2001**, *409*, 422.
(7) Weinacht, T. C.; Bucksbaum, P. H. *J. Opt. B: Quantum Semiclassical Opt.* **2002**, *4*, R35.
(8) Brixner, T.; Gerber, G. *ChemPhysChem* **2003**, *4*, 418.
(9) Dantus, M.; Lozovoy, V. V. *Chem. Rev.* **2004**, *104*, 1813.
(10) Lozovoy, V. V.; Dantus, M. *Annu. Rep. Prog. Chem., Sect. C* **2006**, *102*, 227.
(11) Ohmori, K. *Annu. Rev. Phys. Chem.* **2009**, *60*, 487.
(12) Worth, G. A.; Cederbaum, L. S. *Annu. Rev. Phys. Chem.* **2004**, *55*, 127.
(13) Mahapatra, S. *Acc. Chem. Res.* **2008**, *42*, 1004.
(14) Schoenlein, R. W.; Peteanu, L. A.; Mathies, R. A.; Shank, C. V. *Science* **1991**, *254*, 412.
(15) Knox, R. S. *J. Photochem. Photobiol., B* **1999**, *49*, 81.
(16) Sundström, V. *Prog. Quantum Electron.* **2000**, *24*, 187.
(17) Kukura, P.; McCamant, D. W.; Yoon, S.; Wandschneider, D. B.; Mathies, R. A. *Science* **2005**, *310*, 1006.
(18) Sundström, V. *Annu. Rev. Phys. Chem.* **2008**, *59*, 53.
(19) Polanyi, J. C.; Wong, W. H. *J. Chem. Phys.* **1969**, *51*, 1439.
(20) Levine, R. D. *Molecular Reaction Dynamics*; Cambridge University Press: New York, 2005.
(21) Vallance, C. *Phil. Trans. R. Soc. London, Ser. A* **2004**, *362*, 2591.

(22) Ashfold, M. N. R.; Nahler, H. N.; Orr-Ewing, A. J.; Vieuxmaire, O. P. J.; Toomes, R. L.; Kitsopoulos, T. N.; Garcia, I. A.; Chestakov, D. A.; Wu, S.-M.; Parker, D. H. *Phys. Chem. Chem. Phys.* **2006**, *8*, 26.
(23) Simons, J. P. *J. Phys. Chem.* **1987**, *91*, 5378.
(24) Houston, P. L. *J. Phys. Chem.* **1987**, *91*, 5388.
(25) Hall, G. E.; Houston, P. L. *Annu. Rev. Phys. Chem.* **1989**, *40*, 375.
(26) Houston, P. L. *Acc. Chem. Res.* **1989**, *22*, 309.
(27) Alexander, A. J.; Zare, R. N. *Acc. Chem. Res.* **2000**, *33*, 199.
(28) Clark, A. P.; Brouard, M.; Quadrini, F.; Vallance, C. *Phys. Chem. Chem. Phys.* **2006**, *8*, 5591.
(29) Suits, A. G.; Vasyutinskii, O. S. *Chem. Rev.* **2008**, *108*, 3706.
(30) Seideman, T. *Phys. Rev. A* **2001**, *64*, 042504.
(31) Seideman, T. *Annu. Rev. Phys. Chem.* **2002**, *53*, 41.
(32) Stolow, A.; Bragg, A. E.; Neumark, D. M. *Chem. Rev.* **2004**, *104*, 1719.
(33) Suzuki, T. *Annu. Rev. Phys. Chem.* **2006**, *57*, 555.
(34) Continetti, R. E. *Annu. Rev. Phys. Chem.* **2001**, *52*, 165.
(35) Davies, J. A.; LeClaire, J. E.; Continetti, R. E.; Hayden, C. C. *J. Chem. Phys.* **1999**, *111*, 1.
(36) Davies, J. A.; Continetti, R. E.; Chandler, D. W.; Hayden, C. C. *Phys. Rev. Lett.* **2000**, *84*, 5983.
(37) Rijs, A. M.; Janssen, M. H. M.; Chrysostom, E. t.-H.; Hayden, C. C. *Phys. Rev. Lett.* **2004**, *92*, 123002.
(38) Gessner, O.; Lee, A. M. D.; Shaffer, J. P.; Reisler, H.; Levchenko, S. V.; Krylov, A. I.; Underwood, J. G.; Shi, H.; East, A. L. L.; Wardlaw, D. M.; Chrysostom, E. t.-H.; Hayden, C. C.; Stolow, A. *Science* **2006**, *311*, 219.
(39) Vredenborg, A.; Roeterdink, W. G.; Janssen, M. H. M. *J. Chem. Phys.* **2008**, *128*, 204311.
(40) Vredenborg, A.; Roeterdink, W. G.; de Lange, C. A.; Janssen, M. H. M. *Chem. Phys. Lett.* **2009**, *478*, 20.
(41) Parker, D. H.; Bernstein, R. B. *Annu. Rev. Phys. Chem.* **1989**, *40*, 561.
(42) Bulthuis, J.; van Leuken, J. J.; Stolte, S. *Faraday Trans.* **1995**, *91*, 205.
(43) Loesch, H. J. *Annu. Rev. Phys. Chem.* **1995**, *46*, 555.
(44) Aquilanti, V.; Bartolomei, M.; Pirani, F.; Cappelletti, D.; Vecchiocattivi, F.; Shimizu, Y.; Kasai, T. *Phys. Chem. Chem. Phys.* **2005**, *7*, 291.
(45) Stern, W.; Gerlach, W. *Z. Phys.* **1921**, *8*, 110.
(46) Bethlem, H. L.; Meijer, G. *Int. Rev. Phys. Chem.* **2003**, *22*, 73.
(47) Schnell, M.; Meijer, G. *Angew. Chem., Int. Ed.* **2009**, *48*, 6010.
(48) Bell, M. T.; Softley, T. P. *Mol. Phys.* **2009**, *107*, 99.
(49) Townsend, D.; Goodgame, A. L.; Procter, S. R.; Mackenzie, S. R.; Softley, T. P. *J. Phys. B: At. Mol. Opt. Phys.* **2001**, *34*, 439.
(50) Yamakita, Y.; Procter, S. R.; Goodgame, A. L.; Softley, T. P.; Merkt, F. *J. Chem. Phys.* **2004**, *121*, 1419.
(51) Vliegen, E.; Wörner, H. J.; Softley, T. P.; Merkt, F. *Phys. Rev. Lett.* **2004**, *92*, 033005.
(52) Softley, T. P.; Procter, S. R.; Yamakita, Y.; Maguire, G.; Merkt, F. *J. Electron Spectrosc. Relat. Phenom.* **2005**, *144*, 113.
(53) Stapelfeldt, H.; Sakai, H.; Constant, E.; Corkum, P. B. *Phys. Rev. Lett.* **1997**, *79*, 2787.
(54) Sakai, H.; Tarasevitch, A.; Danilov, J.; Stapelfeldt, H.; Yip, R. W.; Ellert, C.; Constant, E.; Corkum, P. B. *Phys. Rev. A* **1998**, *57*, 2794.
(55) Fulton, R.; Bishop, A. I.; Barker, P. F. *Phys. Rev. Lett.* **2004**, *93*, 243004.
(56) Lamb Jr, W. E. *Phys. Today* **1969**, *22*, 23.
(57) Nesbitt, D. J.; Field, R. W. *J. Phys. Chem.* **1996**, *100*, 12735.
(58) Boyall, D.; Reid, K. L. *Chem. Soc. Rev.* **1997**, *26*, 223.
(59) Shapiro, M.; Brumer, P. *J. Chem. Phys.* **1986**, *84*, 4103.
(60) Zhu, L.; Suto, K.; Fiss, J. A.; Wada, R.; Seideman, T.; Gordon, R. J. *Phys. Rev. Lett.* **1997**, *79*, 4108.
(61) Tannor, D. J.; Rice, S. A. *J. Chem. Phys.* **1985**, *83*, 5013.
(62) Bergmann, K.; Theuer, H.; Shore, B. W. *Rev. Mod. Phys.* **1998**, *70*, 1003.
(63) Judson, R. S.; Rabitz, H. *Phys. Rev. Lett.* **1992**, *68*, 1500.
(64) Lozovoy, V. V.; Dantus, M. *ChemPhysChem* **2005**, *6*, 1970.
(65) Cornaggia, C.; Lavancier, D.; Normand, D.; Morellec, J.; Liu, H. X. *Phys. Rev. A* **1990**, *42*, 5464.
(66) Constant, E.; Stapelfeldt, H.; Corkum, P. B. *Phys. Rev. Lett.* **1996**, *76*, 4140.
(67) Lezius, M.; Blanchet, V.; Rayner, D. M.; Villeneuve, D. M.; Stolow, A.; Ivanov, M. Y. *Phys. Rev. Lett.* **2001**, *86*, 51.
(68) Frasinski, L. J.; Codling, K.; Hatherly, P.; Barr, J.; Ross, I. N.; Toner, W. T. *Phys. Rev. Lett.* **1987**, *58*, 2424.
(69) Garraway, B. M.; Suominen, K.-A. *Phys. Rev. Lett.* **1998**, *80*, 932.
(70) Solá, I. R.; Chang, B. Y.; Santamaria, J.; Malinovsky, V. S.; Krause, J. L. *Phys. Rev. Lett.* **2000**, *85*, 4241.
(71) Solá, I. R. *Phys. Rev. A* **2004**, *69*, 033401.
(72) Bandrauk, A. D.; Sink, M. L. *J. Chem. Phys.* **1981**, *74*, 1110.
(73) George, T. F.; Zimmerman, I. H.; Yuan, J.-M.; Laing, J. R.; DeVries, P. L. *Acc. Chem. Res.* **1977**, *10*, 449.
(74) Zavriyev, A.; Bucksbaum, P. H.; Muller, H. G.; Schumacher, D. W. *Phys. Rev. A* **1990**, *42*, 5500.
(75) Frasinski, L. J.; Posthumus, J. H.; Plumridge, J.; Codling, K.; Taday, P. F.; Langley, A. J. *Phys. Rev. Lett.* **1999**, *83*, 3625.
(76) Niikura, H.; Corkum, P. B.; Villeneuve, D. M. *Phys. Rev. Lett.* **2003**, *90*, 203601.
(77) Han, Y.-C.; Yuan, K.-J.; Hu, W.-H.; Cong, S.-L. *J. Chem. Phys.* **2009**, *130*, 044308.
(78) Underwood, J. G.; Spanner, M.; Ivanov, M. Y.; Mottershead, J.; Sussman, B. J.; Stolow, A. *Phys. Rev. Lett.* **2003**, *90*, 223001.
(79) Sussman, B. J.; Underwood, J. G.; Lausten, R.; Ivanov, M. Y.; Stolow, A. *Phys. Rev. A* **2006**, *73*, 053403.
(80) Sussman, B. J.; Ivanov, M. Y.; Stolow, A. *Phys. Rev. A* **2005**, *71*, 051401.
(81) Sussman, B. J.; Townsend, D.; Ivanov, M. Y.; Stolow, A. *Science* **2006**, *314*, 278.
(82) Reim, K. F.; Nunn, J.; Lorenz, V. O.; Sussman, B. J.; Lee, K. C.; Langford, N. K.; Jaksch, D.; Walmsley, I. A. *Nat. Photonics* **2010**, *4*, 218.
(83) Stark, J. *Ann. Phys.* **1914**, *43*, 965.
(84) Zeeman, P. *Nature* **1897**, *55*, 347.
(85) Goodgame, A. L.; Softley, T. P. *J. Phys. B: At. Mol. Opt. Phys.* **1999**, *32*, 4839.
(86) Sussman, B. J. *Am. J. Phys.*, in print.
(87) Stolow, A.; Underwood, J. G. *Adv. Chem. Phys.* **2008**, *139*, 497.
(88) Edmonds, A. R. *Angular Momentum in Quantum Mechanics*; Princeton University Press: Princeton, NJ, 1957.
(89) Zare, R. N. *Angular Momentum: Understanding Spatial Aspects in Chemistry and Physics*; John Wiley & Sons: New York, 1988.
(90) Zare, R. N.; Herschbach, D. R. *Proc. IEEE* **1963**, *51*, 173.
(91) Zare, R. N. *Mol. Photochem.* **1972**, *4*, 1.
(92) Stapelfeldt, H.; Constant, E.; Corkum, P. B. *Phys. Rev. Lett.* **1995**, *74*, 3780.
(93) Stapelfeldt, H.; Constant, E.; Sakai, H.; Corkum, P. B. *Phys. Rev. A* **1998**, *58*, 426.
(94) Larsen, J. J.; Sakai, H.; Safvan, C. P.; Wendt-Larsen, I.; Stapelfeldt, H. *J. Chem. Phys.* **1999**, *111*, 7774.
(95) Friedrich, B.; Herschbach, D. *Phys. Rev. Lett.* **1995**, *74*, 4623.
(96) Seideman, T. *J. Chem. Phys.* **1995**, *103*, 7887.
(97) Stapelfeldt, H.; Seideman, T. *Rev. Mod. Phys.* **2003**, *75*, 543.
(98) Ortigoso, J.; Rodriguez, M.; Gupta, M.; Friedrich, B. *J. Chem. Phys.* **1999**, *110*, 3870.
(99) Rosca-Pruna, F.; Vrakking, M. J. J. *Phys. Rev. Lett.* **2001**, *87*, 153902.
(100) Barnett, S. M.; Pegg, D. T. *Phys. Rev. A* **1990**, *41*, 3427.
(101) Franke-Arnold, S.; Barnett, S. M.; Yao, E.; Leach, J.; Courtial, J.; Padgett, M. *New J. Phys.* **2004**, *6*, 103.
(102) Litvinyuk, I. V.; Lee, K. F.; Dooley, P. W.; Rayner, D. M.; Villeneuve, D. M.; Corkum, P. B. *Phys. Rev. Lett.* **2003**, *90*, 233033.
(103) Leibscher, M.; Averbukh, I. S.; Rabitz, H. *Phys. Rev. Lett.* **2003**, *90*, 213001.
(104) Lee, K. F.; Litvinyuk, I. V.; Dooley, P. W.; Spanner, M.; Villeneuve, D. M.; Corkum, P. B. *J. Phys. B: At. Mol. Opt. Phys.* **2004**, *37*, L43.
(105) Bisgaard, C. Z.; Viftrup, S. S.; Stapelfeldt, H. *Phys. Rev. A* **2006**, *73*, 053410.
(106) Bisgaard, C. Z.; Poulsen, T. B.; Peronne, E.; Viftrup, S. S.; Stapelfeldt, H. *Phys. Rev. Lett.* **2004**, *92*, 173004.
(107) Cryan, J. P.; Bucksbaum, P. H.; Coffee, R. N. *Phys. Rev. A* **2009**, *80*, 063412.
(108) Spanner, M.; Shapiro, E. A.; Ivanov, M. *Phys. Rev. Lett.* **2004**, *92*, 093001.
(109) Renard, M.; Hertz, E.; Guérin, S.; Jauslin, H. R.; Lavorel, B.; Faucher, O. *Phys. Rev. A* **2005**, *72*, 025401.
(110) Fleischer, S.; Averbukh, I. S.; Prior, Y. *Phys. Rev. A* **2006**, *74*, 041403.
(111) Li, X.; Liu, P.; Zhao, S.; Zeng, Z.; Li, R.; Xu, Z. *Chem. Phys. Lett.* **2009**, *475*, 183.
(112) Suzuki, T.; Sugawara, Y.; Minemoto, S.; Sakai, H. *Phys. Rev. Lett.* **2008**, *100*, 033603.
(113) Bisgaard, C. Z.; Clarkin, O. J.; Wu, G. R.; Lee, A. M. D.; Gessner, O.; Hayden, C. C.; Stolow, A. *Science* **2009**, *323*, 1464.
(114) Townsend, D.; Satzger, H.; Ejdrup, T.; Lee, A. M. D.; Stapelfeldt, H.; Stolow, A. *J. Chem. Phys.* **2006**, *125*, 234302.
(115) Velotta, R.; Hay, N.; Mason, M. B.; Castillejo, M.; Marangos, J. P. *Phys. Rev. Lett.* **2001**, *87*, 183901.
(116) Kaku, M.; Masuda, K.; Miyazaki, A. *Jpn. J. Appl. Phys., Part 2* **2004**, *43*, L591.
(117) Itatani, J.; Zeidler, D.; Levesque, J.; Spanner, M.; Villeneuve, D. M.; Corkum, P. B. *Phys. Rev. Lett.* **2005**, *94*, 123902.
(118) Itatani, J.; Levesque, J.; Zeidler, D.; Niikura, H.; Kieffer, J. C.; Corkum, P. B.; Villeneuve, D. M. *Nature* **2004**, *432*, 867.

(119) Fleischer, S.; Averbukh, I. S.; Prior, Y. *Phys. Rev. Lett.* **2007**, *99*, 093002.
(120) Karczmarek, J.; Wright, J.; Corkum, P. B.; Ivanov, M. Y. *Phys. Rev. Lett.* **1999**, *82*, 3420.
(121) Villeneuve, D. M.; Aseyev, S. A.; Dietrich, P.; Spanner, M.; Ivanov, M. Y.; Corkum, P. B. *Phys. Rev. Lett.* **2000**, *85*, 542.
(122) Hasbani, R.; Ostojić, B.; Bunker, P. R.; Ivanov, M. Y. *J. Chem. Phys.* **2002**, *116*, 10636.
(123) Comstock, M.; Senekerimyan, V.; Dantus, M. *J. Phys. Chem. A* **2003**, *107*, 8271.
(124) Rouzée, A.; Renard, M.; Guérin, S.; Faucher, O.; Lavorel, B. *Phys. Rev. A* **2007**, *75*, 013419.
(125) Mairesse, Y.; Zeidler, D.; Dudovich, N.; Spanner, M.; Levesque, J.; Villeneuve, D. M.; Corkum, P. B. *Phys. Rev. Lett.* **2008**, *100*, 143903.
(126) Goban, A.; Minemoto, S.; Sakai, H. *Phys. Rev. Lett.* **2008**, *101*, 013001.
(127) Renard, V.; Renard, M.; Guérin, S.; Pashayan, Y. T.; Lavorel, B.; Faucher, O.; Jauslin, H. R. *Phys. Rev. Lett.* **2003**, *90*, 153601.
(128) Herzberg, G. *Molecular Spectra & Molecular Structure Vol. III — Electronic Spectra & Electronic Structure of Polyatomic Molecules*; Van Nostrand: New York, 1966.
(129) Larsen, J. J.; Hald, K.; Bjerre, N.; Stapelfeldt, H. *Phys. Rev. Lett.* **2000**, *85*, 2470.
(130) Daems, D.; Guérin, S.; Hertz, E.; Jauslin, H. R.; Lavorel, B.; Faucher, O. *Phys. Rev. Lett.* **2005**, *95*, 063005.
(131) Hertz, E.; Daems, D.; Guérin, S.; Jauslin, H. R.; Lavorel, B.; Faucher, O. *Phys. Rev. A* **2007**, *76*, 043423.
(132) Rouzée, A.; Guérin, S.; Faucher, O.; Lavorel, B. *Phys. Rev. A* **2008**, *77*, 043412.
(133) Underwood, J. G.; Sussman, B. J.; Stolow, A. *Phys. Rev. Lett.* **2005**, *94*, 143002.
(134) Viftrup, S. S.; Kumarappan, V.; Trippel, S.; Stapelfeldt, H.; Hamilton, E.; Seideman, T. *Phys. Rev. Lett.* **2007**, *99*, 143602.
(135) Lee, K. F.; Villeneuve, D. M.; Corkum, P. B.; Stolow, A.; Underwood, J. G. *Phys. Rev. Lett.* **2006**, *97*, 173001.
(136) Bustard, P. J.; Sussman, B. J.; Walmsley, I. A. *Phys. Rev. Lett.* **2010**, *104*, 193902.
(137) Ghafur, G.; Rouzée, A.; Gijsbertsen, A.; Siu, W. K.; Stolte, S.; Vrakking, M. J. J. *Nat. Phys.* **2009**, *5*, 289.
(138) Filsinger, F.; Küpper, J.; Meijer, G.; Holmegaard, L.; Nielsen, J. H.; Nevo, I.; Hansen, J. L.; Stapelfeldt, H. *J. Chem. Phys.* **2009**, *131*, 064309.
(139) Shore, B. W. *Acta Phys. Slovaca* **2008**, *58*, 243.
(140) González-Vázquez, J.; Solá, I. R.; Santamaria, J.; Malinovsky, V. S. *J. Chem. Phys.* **2006**, *125*, 124315.
(141) Choi, H.; Son, W.-J.; Shin, S.; Chang, B. Y.; Solá, I. R. *J. Chem. Phys.* **2008**, *128*, 104315.
(142) Chang, B. Y.; Choi, H.; Shin, S.; Lee, S.; Solá, I. R. *J. Mod. Opt.* **2009**, *56*, 811.
(143) Chang, B. Y.; Shin, S.; Santamaria, J.; Solá, I. R. *J. Chem. Phys.* **2009**, *130*, 124320.
(144) Zener, C. *Proc. R. Soc. London, Ser. A* **1932**, *137*, 696.
(145) Landau, L. D. *Phys. Z.* **1932**, *2*, 46.
(146) Wittig, C. *J. Phys. Chem. B* **2004**, *109*, 8428.
(147) Wrede, E.; Laubach, S.; Schulenburg, S.; Brown, A.; Wouters, E. R.; Orr-Ewing, A. J.; Ashfold, M. N. R. *J. Chem. Phys.* **2001**, *114*, 2629.
(148) Shapiro, M.; Bony, H. *J. Chem. Phys.* **1985**, *83*, 1588.
(149) Eppink, A. T. J. B.; Parker, D. H. *J. Chem. Phys.* **1998**, *109*, 4758.
(150) Eppink, A. T. J. B.; Parker, D. H. *Rev. Sci. Instrum.* **1997**, *68*, 3477.
(151) Rakitzis, T. P.; Kandel, S. A.; Alexander, A. J.; Kim, Z. H.; Zare, R. N. *Science* **1998**, *281*, 1346.
(152) Rakitzis, T. P.; Kandel, S. A.; Zare, R. N. *J. Chem. Phys.* **1998**, *108*, 8291.
(153) Tauber, M. J.; Mathies, R. A.; Chen, X.; Bradforth, S. E. *Rev. Sci. Instrum.* **2003**, *74*, 4958.
(154) Lvovsky, A. I.; Sanders, B. C.; Tittel, W. *Nat. Photonics* **2009**, *3*, 706.
(155) Nunn, J.; Reim, K.; Lee, K. C.; Lorenz, V. O.; Sussman, B. J.; Walmsley, I. A.; Jaksch, D. *Phys. Rev. Lett.* **2008**, *101*, 260502.
(156) Nunn, J.; Walmsley, I. A.; Raymer, M. G.; Surmacz, K.; Waldermann, F. C.; Wang, Z.; Jaksch, D. *Phys. Rev. A* **2007**, *75*, 011401.

JP109095D